Facile C-H bond cleavage via a proton coupled electron transfer involving a C-H•••Cu^{II} interaction

Xavi Ribas,* Carlos Calle, Albert Poater, Alicia Casitas, Laura Gómez, Raül Xifra, Teodor Parella, Jordi Benet-Buchholz, Arthur Schweiger, George Mitrikas,* Miquel Solà,* Antoni Llobet,* T. Daniel P. Stack*

CONTENTS

1. SUPPLEMENTARY METHODS

Ligands H33m, D-H33m and pNO$_2$-H33m were synthesized following published procedures,[1,2,3] and characterization of complex 2 was performed accordingly to previous work.[1] All chemicals were obtained from Aldrich unless indicated otherwise, and were used without further purification. Solvents from SDS were dried in a MBraun SPS800 solvent purification system. Butyronitrile (Fluka, 99.0 %) was used for EPR experiments without further purification.

1.1. Instrumentation and measurements

IR spectra were recorded on a Mattson Satellite FT-IR using a MKII Golden Gate Single Reflection ATR System. UV-vis spectroscopy was performed on a Cary 50 Scan (Varian) UV-vis spectrophotometer. Low temperature control was maintained with a cryostat from Unisoku Scientific Instruments, Japan. NMR data were collected on Bruker 600, Bruker 500 or Bruker 400 AVANCE spectrometers in CDCl$_3$ or D3-acetonitrile and calibrated relative to an internal reference, either the residual protons of the solvent or added tetramethylsilane. C, H, N elemental analyses were performed on a Fison EA-1108 analyzer. ESI-MS experiments were collected and analyzed on a Bruker Daltonics Esquire 3000 spectrometer with acetonitrile as the mobile phase. EPR equipment detailed in section 1D.

1.2. Synthetic procedures

[Cu^{II}(H33m)](CF$_3$SO$_3$)$_2$, 1•(CF$_3$SO$_3$)$_2$ and [Cu^{II}(D-H33m)](CF$_3$SO$_3$)$_2$: Acetonitrile (CH$_3$CN) solutions of equimolar amounts of the H33m or the mono-deuterated H33m ligand and Cu^{II}(CF$_3$SO$_3$)$_2$ each were cooled to 233 K (CH$_3$CN/liquid-N$_2$ (LN$_2$)) and mixed

to form a green solution. UV-vis (CH$_3$CN): λ_{max} (ε) = 272 (4060), 324 (8500), 425 (960), 640 nm (185 M^{-1}·cm^{-1}). The calculated extinction coefficients assumed a quantitative formation of the 1:1 complex and the solvent volume measured at 298 K.

[Ni^{II}(H33m)(CH$_3$CN)](ClO$_4$)$_2$, 3•(ClO$_4$)$_2$. Acetonitrile solutions of equimolar amounts of H33m and Ni^{II}(ClO$_4$)$_2$·6H$_2$O were mixed at 298 K to give a green solution. UV-vis (CH$_3$CN): λ_{max} (ε) = 325 (sh, 180), 385 (sh, 92), 600 nm (27 M^{-1}·cm^{-1}). The calculated extinction coefficients of **3** assumed a quantitative formation of the 1:1 complex and the solvent volume measured at 298 K. ^{1}H-NMR (600 MHz, CD$_3$CN, 248 K, paramagnetic spectrum): broad signals at 418, 255, 241, 85, 60, 51, 46, 44, 17, -8, -16, -19 ppm. Peaks in the 0-8 ppm range corrrespond to free ligand (<20%). An similar UV-Vis and ^{1}H-NMR spectrum was obtained for complex, [Ni^{II}(D-H33m)(CH$_3$CN)](ClO$_4$)$_2$ (Fig. S7).

[Ni^{II}-aryl](NO$_3$), 4•(NO$_3$): Equimolar amounts of H33m (11.5 mg, 0.049 mmols) and Ni^{II}(NO$_3$)$_2$·6H$_2$O (14.3 mg, 0.049 mmols) were mixed and stirred in 2 mL of CH$_3$CN overnight. After filtering, diethyl ether was diffused slowly allowing for the formation of X-ray diffraction quality crystals in a 55% yield (11.3 mg, 0.027 mmols). UV-vis (CH$_3$CN): λ_{max} (ε) = 425 (439), 484 nm (sh, 125 M^{-1}·cm^{-1}). ESI-MS (CH$_3$CN): 290 [Ni^{II}(H33m-C)]$^+$. X-Ray Diffraction details in Table S1. A similar procedure using Ni^{II}(ClO$_4$)$_2$ yielded **4•(ClO$_4$)**. ^{1}H-NMR (600 MHz, CD$_3$CN, 298 K): δ = 6.96 (t, 1H), 6.69 (d, 2H), 4,10 (m, 2H), 3.67 (m, 2H), 2.70 (m, 4H), 2.65 (m, 2H), 2.53 (m, 2H), 1,80 (m, 2H), 1,42 (m, 2H). ^{13}C-NMR (150 MHz, CD$_3$CN, 298 K): δ = 124.9, 117.8, 62.9, 50.8, 50.8, 26.8.

1.3. Sample preparation for EPR studies

[Cu^{II}(H33m)](CF$_3$SO$_3$)$_2$, 1·(CF$_3$SO$_3$)$_2$: Equimolar amounts of H33m (8.41 mg, 36 µmol) and Cu^{II}(CF$_3$SO$_3$)$_2$ were dissolved in butyronitrile (1.5 ml and 0.5 ml. respectively) at room temperature. Before mixing, each solution was cooled to 233 K (CH$_3$CN/LN$_2$). The resulting intense green solution was stirred for 3 min., after which ca. 120 µl were transferred to a pre-cooled (193 K) X-band EPR sample tube, which was immediately placed into LN$_2$ yielding a green colored glass. The sample tube was kept frozen throughout the EPR experiments.

[Cu^{II}(D-H33m)](CF$_3$SO$_3$)$_2$: A similar procedure was followed to prepare the mono-deuterated analogue using D-H33m (9.40 mg, 40 µmol) and Cu^{II}(CF$_3$SO$_3$)$_2$ (14.50 mg, 40 µmol) in butyronitrile.

1.4. EPR spectroscopy details

Continuous wave (cw) EPR measurements at X-band were performed on a Bruker E500 spectrometer equipped with a super-high Q cavity. Experimental conditions: mw frequency, 9.495 GHz; mw power incident to the cavity, 0.2 mW; modulation frequency, 100 kHz; modulation amplitude, 0.1 mT. Sample cooling was achieved using a LN$_2$ dewar (120 K).

Pulse EPR measurements at X-band (mw frequency 9.748 GHz) were performed on a Bruker E580 spectrometer at 15 K. The field-swept EPR spectrum was recorded via the FID following a pulse length of 500 ns. Davies-ENDOR experiments were carried out with a pulse sequence of π - T - $\pi/2$ - τ - π - τ - echo with a $\pi/2$ pulse of length 16 ns, a radio frequency pulse of length 10 μs and either a waiting time τ between the pulses

of 200 ns or a more selective sequence with a $\pi/2$ pulse of length 200 ns and τ of 500 ns.

HYSCORE spectroscopy with the pulse sequence $\pi/2 - \tau - \pi/2 - t_1 - \pi - t_2 - \pi/2 - \tau$ - echo were carried out with the following instrumental parameters: $t_{\pi/2} = t_\pi = 16$ ns; starting values of the two variable times t_1 and t_2, 96 ns; time increment, $\Delta t = 16$ ns (data matrix 400 x 400); in order to eliminate blind-spot artifacts, up to seven spectra were recorded with $\tau = 100, 118, 136, 160, 178, 240$ and 360 ns for $[Cu^{II}(H33m)](CF_3SO_3)_2$ and three with $\tau = 100, 140, 168$ ns for $[Cu^{II}(D\text{-}H33m)](CF_3SO_3)_2$ and summed up. An eight-step phase cycle was used to remove unwanted echoes.

The data were processed with the program MATLAB 7.0 (The MathWorks, Natick, MA). The HYSCORE time traces were baseline corrected with a second-order exponential, apodized with a gaussian window and zero filled. After a two-dimensional Fourier transform the absolute-value spectra were calculated. The experimental cw EPR spectra were simulated using the EasySpin package.[4] The HYSCORE spectra were simulated with a custom program,[5] taking into account peak amplitudes.

1.5. Computational details

All geometry optimizations were performed at the B3LYP level,[6,7,8] with a standard 6-31++G(d,p) basis set[9] in the Gaussian03 package (Table S2-S3).[10] The complete list of authors for *reference 31* in the main text corresponds to ref 10 in this Supplorting Information document. The geometry optimizations were performed without symmetry constraints and were checked by analytical frequency calculations. Solvent effects including contributions of non electrostatic terms were estimated in single point calculations on the gas phase optimized structures, based on the polarizable continuous

solvation model PCM using CH_3CN as a solvent.[11] The solvent effect was introduced by the conductor polarizable calculation model (CPCM).[11,12] The cavity was created via a series of overlapping spheres. Solvent effects were also considered in Time-Dependent DFT (TD-DFT) on **1** and **3**. Natural bond orbital (NBO) analysis[13] at the same level of theory provided a quantitative picture of the sigma interaction in terms of the second order delocalization energy correction (Table S2).

In addition, local aromaticity changes have been quantified using two probes of local aromaticity based on structure and magnetic properties, respectively. As a structure-based measure of aromaticity, we have employed the harmonic oscillator model of aromaticity (HOMA) index (Eq. S1), defined by Kruszewski and Krygowski as:[14]

$$HOMA = 1 - \frac{\alpha}{n}\sum_{i=1}^{n}\left(R_{opt} - R_i\right)^2 , \text{(Eq. S1)}$$

where n is the number of bonds considered, and α is an empirical constant (for CC bonds $\alpha = 257.7$) fixed to give HOMA = 0 for a model nonaromatic system, and HOMA = 1 for a system with all bonds equal to an optimal value R_{opt}, which is 1.388 Å for C-C bonds, assumed to be achieved for fully aromatic systems. R_i stands for a running bond length. This index was found to be one of the most effective structural indicators of aromaticity.[15] As a magnetic index of aromaticity, we have used the nucleus-independent chemical shift (NICS) measures proposed by Schleyer and co-workers.[16] This is one of the most widely employed indicators of aromaticity. It is defined as the negative value of the absolute shielding computed at a ring centre or at some other interesting point of the system. Rings with large negative NICS values are considered

aromatic. The more negative the NICS values, the more aromatic the rings are. NICS(1) values estimated at 1 Å above the centre of the ring have been also computed.[17]

Based on the optimized geometry of **1,** spin-unrestricted DFT calculations were performed with the Amsterdam Density Functional (ADF 2006.01) package.[18] The calculation of the hyperfine parameters was performed with the BPW91 functional[19] and an all-electron triple-ζ basis set with double polarization functions (TZ2P) with the scalar relativistic zero-order regular approximation (ZORA) method.[20]

Calculations have been performed on $[Cu^{II}(H33m)]^{2+}$ (**1**) and $[Ni^{II}(H33m)(CH_3CN)]^{2+}$ (**3**) (Table S3). Compound **1** is clearly stable in a doublet ground state, with the quadruplet state lying 75 kcal/mol above in energy. Complex **3** is 6.2 kcal/mol more stable in the triplet ground state compared to the singlet ground state, which agrees with the experimental paramagnetic ^{1}H-NMR spectrum (Figure S8), suggesting a non-square planar d^8-high spin Ni^{II} species.[21] Indeed, calculations on the transition state (TS) for the reaction of **1** and TEMPO with and without a water molecule assisting the reaction have been performed (Figure 5 main text, xyz coordinates in Table S3), and both TS are more stable as a singlet biradical.

1.6. X-ray diffraction measurements

Crystal structure measurement of complex **4**•(NO_3) was performed at 153(2) K on a *BRUKER SMART APEX CCD* diffractometer using graphite-monochromated Mo *K*α radiation (λ = 0.71073 Å) from an X-Ray Tube (Table S1). The measurements were made in the range 2.27 to 31.53° for θ. Full-sphere data collection was carried out with ω and φ scans. A total of 22905 reflections were collected of which 4890 [R_{int} =

0.0566] were unique. The structure was solved by direct methods and refined by full-matrix least-squares methods on F^2. All non-hydrogen atoms were refined anisotropically. The H-atoms were placed in geometrically optimized positions and forced to ride on the atom to which they are attached. Programs used: data collection, Smart version 5.631 (Bruker AXS 1997-02); data reduction, Saint + version 6.36A (Bruker AXS 2001); absorption correction, SADABS version 2.10 (Bruker AXS 2001). Structure solution and refinement was done using SHELXTL Version 6.14 (Bruker AXS 2000-2003). Cambridge Crystallographic data Centre (CCDC) deposit number: 726565.

1.7. Kinetic simulations

The decay profiles of **1** under different experimental conditions were monitored by UV-vis spectroscopy, and fitted with the KINTECUS program.[22] The best fitting of the experimental data trends was achieved by first obtaining the best constant values set for the five-reaction model (Figure 6 in the main text) for the [H33m]/[Cu^{II}] molar ratio of 1.0/2.0 ([H33m]=1.25mM). Constants k_{-1}, k_{-2} and k_{-3} were allowed to vary while the remaining variables were fixed ($k_1 = 1.8 \cdot 10^{+5}$ $M^{-1}s^{-1}$, $k_2 = 1.8 \cdot 10^{+4}$ $M^{-1}s^{-1}$, $k_3 = 6.0$ $M^{-1}s^{-1}$, $k_4 = 8.0 \cdot 10^{+3}$ $M^{-1}s^{-1}$, $k_5 = 8.5 \cdot 10^{+4}$ $M^{-1}s^{-1}$ and $k_{-5} = 7.3 \cdot 10^{+6}$ $M^{-1}s^{-1}$). The rate constants providing the best fits were $k_{-1} = 7.4 \cdot 10^{-4}$ $M^{-1}s^{-1}$, $k_{-2} = 1.9 \cdot 10^{-5}$ $M^{-1}s^{-1}$, $k_{-3} = 9.1 \cdot 10^{-5}$ $M^{-1}s^{-1}$. The calculated decay profiles of **1** for the remaining [H33m]/[Cu^{II}] molar ratios were obtained without modification of the kinetic constants (Figure 6 of the main text).

2. SUPPLEMENTARY DISCUSSION

2.1. cw–EPR, pulse-EPR and DFT studies on 1·(CF₃SO₃)₂

The experimental cw EPR spectrum of species **1** formed at 233 K is simulated (Figure S1) with two Cu^{II} components in a 3:1 ratio. The major component was fitted with g principal values $g_{\parallel}$ = 2.223 ± 0.001 and $g_{\perp}$= 2.055 ± 0.003, and ^{63}Cu hyperfine couplings $A_{\parallel}$ = (405 ± 5) MHz and $A_{\perp}$= (60 ± 20) MHz (Figure S1), and the minor component with $g_{\parallel}$ = 2.252 ± 0.001, $g_{\perp}$ = 2.036 ± 0.003, and ^{63}Cu hyperfine couplings $A_{\parallel}$ = (480 ± 5) MHz and $A_{\perp}$ = (60 ± 20) MHz (Figure S1). The majority species exhibits a measurable feature assigned as a sigma interaction (vide infra), while the minority species neither exhibits a measurable sigma interaction feature nor corresponds to $Cu^{II}(CF_3SO_3)_2$ in butyronitrile (Figure S1). Cw EPR experiments varying the ligand:Cu^{II} molar ratio indicated that excess Cu^{II} relative to the ligand slightly increases the minority species at the expense of the major species. Under conditions of excess ligand relative to Cu^{II}, the 3:1 major:minor ratio does not appreciably change. The copper disproportionation reaction occurs at higher temperatures, yielding EPR-silent solutions, consistent with Cu^{I} and Cu^{III} products.

X-band Davies-ENDOR experiments were performed at different observer positions by applying the two different setups described in the experimental section (Figure S2). At least one set of nitrogen peaks are observed clearly with hyperfine (hf) couplings ranging from 32 to 40 MHz. Additional strong ^1H hf couplings are visible overlapping with the nitrogen peaks at higher frequencies. The insufficient spectral separation of these peaks motivated HYSCORE experiments. Cw ($g_{\parallel}$ = 2.223 ± 0.001, $g_{\perp}$ = 2.055 ± 0.003; $A_{\parallel}$ = (405 ± 5) MHz, $A_{\perp}$ = (60 ± 20) MHz) and X-band Davies-

ENDOR spectrum of $[Cu^{II}(D-H33m)](CF_3SO_3)_2$ have also been recorded (Figures S3 and S4, respectively).

The origin of the protons contributing to the nearly isotropic hf signals observed in HYSCORE spectra for **1** are consistent with its DFT optimized geometry (Figure 2, main text): these signals arise from a ^{1}H nuclei oriented in the molecular plane bound to one of the carbon atoms attached to the secondary amine group (Figure 1, main text), for which positive isotropic hf interactions between 22 and 27 MHz are found. The HYSCORE spectra at lower magnetic field positions, which probe the minority species observed in cw EPR spectra, do not exhibit the specially shaped ^{1}H nuclei interaction (see main text).

2.2. UV-Vis Kinetic Studies on Cu^{II} / H33m reaction

Systematic kinetic studies probed the reaction rate dependence on copper(II) and H33m concentration under anaerobic and anhydrous conditions in CH_3CN. The rates of decay of **1** are unaffected at 1 atm of O_2, but are slowered down (by a factor of 2) by the addition of water. The 425 nm optical feature that forms upon mixing the H33m and Cu(II) is assigned to species **1**, which decays by a single exponential process under conditions of excess ligand (Figure S5).

Dependence of k_{obs} on $[Cu^{II}]^1$

In order to only vary the $[Cu^{II}]$, 1 equiv. of Cu^{II} is assumed to react with 1 equiv. of H33m yielding **1**. Thus the [excess-H33m] is left constant at 0.375 mM at the three different [Cu] (T = 286 K).

a) [Cu]= 1.25 mM, [H33m-total]= 1.625 mM, [excess-H33m]=0.375 mM
b) [Cu]= 0.625 mM, [H33m-total]= 1.0 mM, [excess-H33m]=0.375 mM
c) [Cu]= 0.31 mM, [H33m-total]= 0.6875 mM, [excess-H33m]=0.375 mM

$[Cu^{II}]$ (mM)	$1/[Cu^{II}]$	k_{obs} (min^{-1})
0.31	3.2258	188.9
0.625	1.6	60.1
0.95	1.0526	16.5
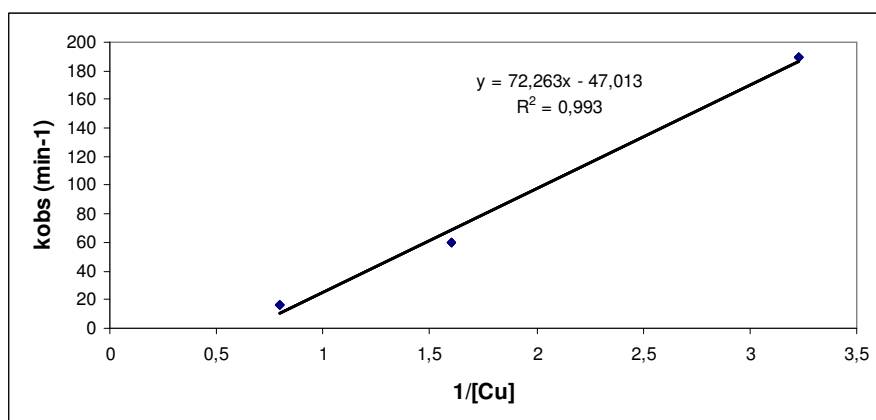
k_{obs} is found to linearly depend on $[Cu^{II}]^{-1}$.

The kinetic model depicted in Figure 6 (main text) predicts a calculated k_{obs} which is also inversely dependent on the $[Cu^{II}]$, albeit with less sensitivity.

$[Cu^{II}]$ (mM)	$1/[Cu^{II}]$	k_{obs} (s^{-1})
0.31	3.2258	5.09
0.625	1.6	4.376
0.95	1.0526	4.125
1.25	0.8	3.925
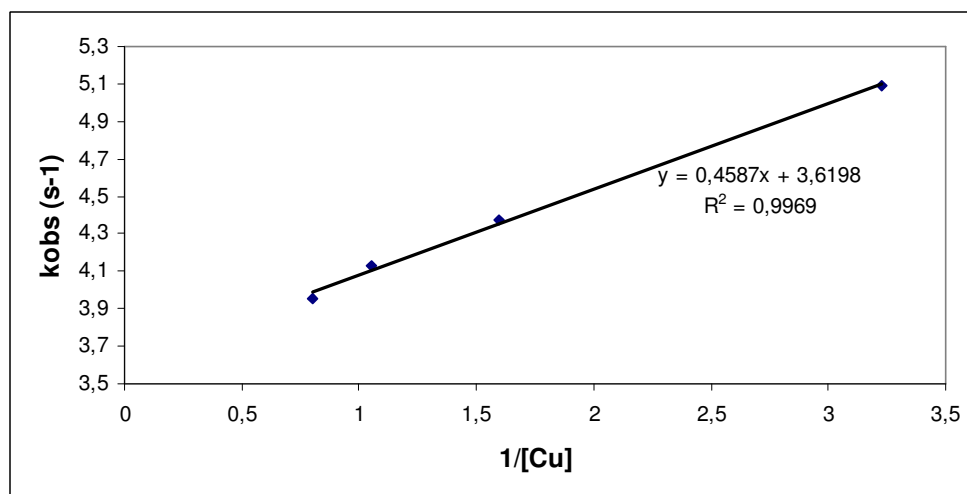
Dependence of k_{obs} on [H33m] (T = 276 K)

    a) [Cu]= 1.25 mM, [H33m-total]= 1.625 mM, [excess-H33m]=0.375 mM
    b) [Cu]= 1.25 mM, [H33m-total]= 1.813 mM, [excess-H33m]=0.5625 mM
    c) [Cu]= 1.25 mM, [H33m-total]= 2.0 mM, [excess-H33m]=0.75 mM

The k_{obs} found with method of initial rates are:

[excess-H33m] (mM)	k_{obs} (s^{-1})
0.375	0.0865
0.5625	0.1383
0.75	0.21
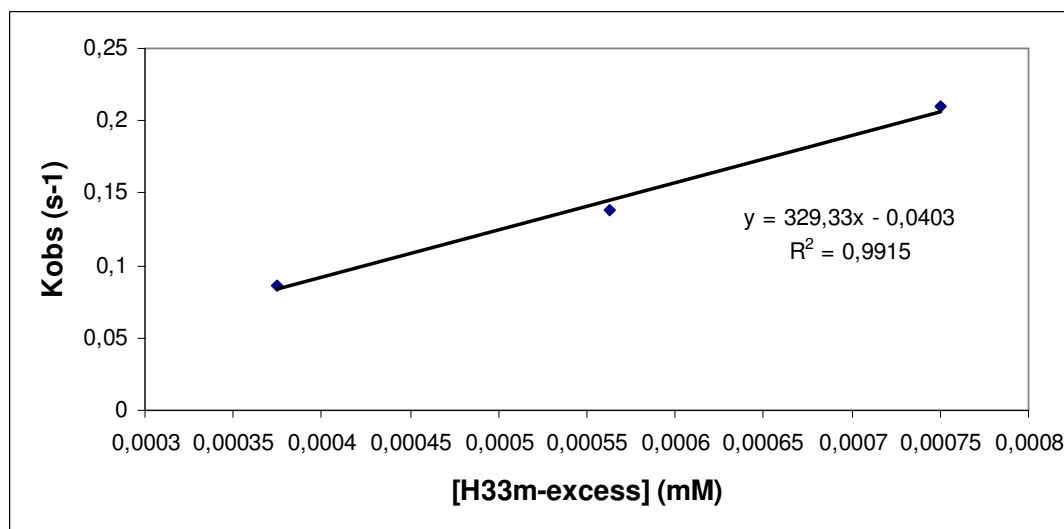
k_{obs} is linearly dependent on [excess-H33m].

The model in Figure 6 (main text) also affords a theoretical k_{obs} dependence on [excess-H33m] :

[H33m] (mM)	[excess-H33m] (mM)	k_{obs} (s^{-1})
1.625	0.375	3.952
1.813	0.5625	6.23
2.0	0.75	8.7
2.75	1.5	20.29

y = 14,706x - 1,9268
R^2 = 0,9979

kobs (s-1)

[H33m-excess] (mM)

25

20

15

10

5

0

0   0,2   0,4   0,6   0,8   1   1,2   1,4   1,6
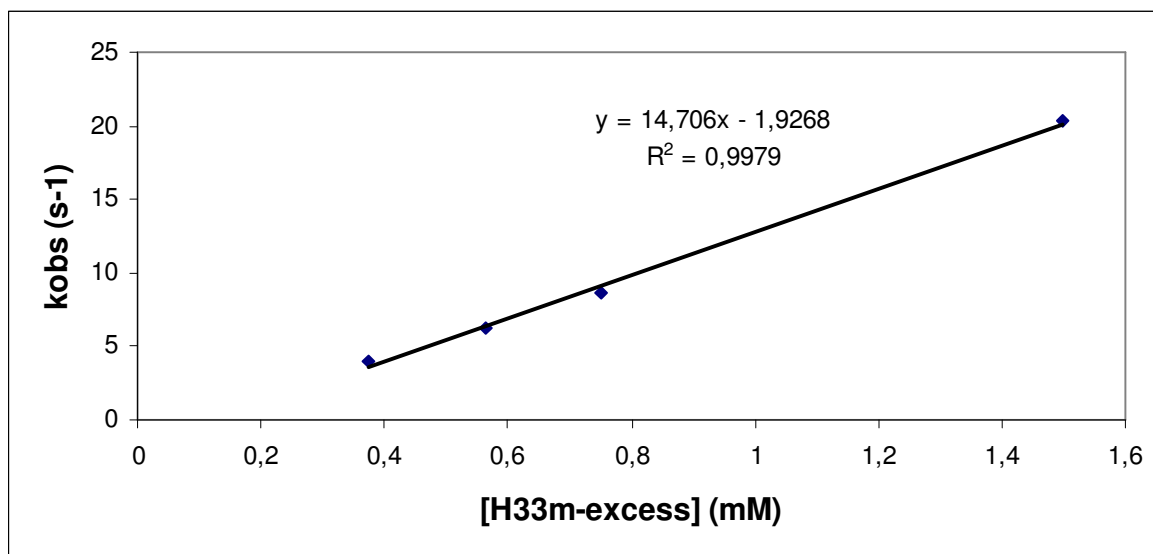
Dependence of k_{obs} on the Ionic Strength (T = 283 K)

The Debye-Huckel limiting law relates k_{obs} with the ionic strength (I) of the solution.[23] A plot of log(k_{obs}) vs $I^{1/2}$ probes the charge of the interacting species at the rate limiting transition state as shown in the following equation:

$$\log(k_{obs}) = \log(k_{obs}^0) + 2\, A\, z_a\, z_b\, I^{1/2}$$

in which A is 1.48 $(mol\ K^{-1})^{-1/2}$ in CH_3CN, and z_a, z_b the charges of the interacting species. A positive slope indicates that either both species interacting in the rate limiting step are either cations or anions, whereas a slope of 0 indicates that neutral species is involved. The decay of the 425 nm band of **1** is appreciable alter with changes in the ionic strengths, modulated by the weakly coordinating counteranion BArF (BArF=tetrakis[(3,5-trifluoromethyl)phenyl]borate, sodium salt, 283 K, anhydrous MeCN, anaerobic). All charged species in solution were included in the calculation of Ionic Strength (I).

a) [Cu]= 1.25 mM, [H33m]= 1.625 mM, [NaBARF]=0 mM
b) [Cu]= 1.25 mM, [H33m]= 1.625 mM, [NaBARF]=8.6 mM
c) [Cu]= 1.25 mM, [H33m]= 1.625 mM, [NaBARF]=16.7 mM
d) [Cu]= 1.25 mM, [H33m]= 1.625 mM, [NaBARF]=20.8 mM
e) [Cu]= 1.25 mM, [H33m]= 1.625 mM, [NaBARF]=33.3 mM

[NaBARF] (mM)	Ionic Strength (I, in molalities)	$I^{1/2}$	k_{obs} (s^{-1})	$\log(k_{obs})$
0	0.004795	0.069249	0.105	-0.978811
8.6	0.015793	0.125670	0.1693	-0.771343
16.67	0.026113	0.161594	0.3212	-0.493224
20.83	0.031432	0.177291	0.3442	-0.463189
33.33	0.047417	0.217754	0.4565	-0.340559

Plot of $\log(k_{obs})$ versus $I^{1/2}$ with linear fit $y = 4.5559x - 1.2942$, $R^2 = 0.9678$.
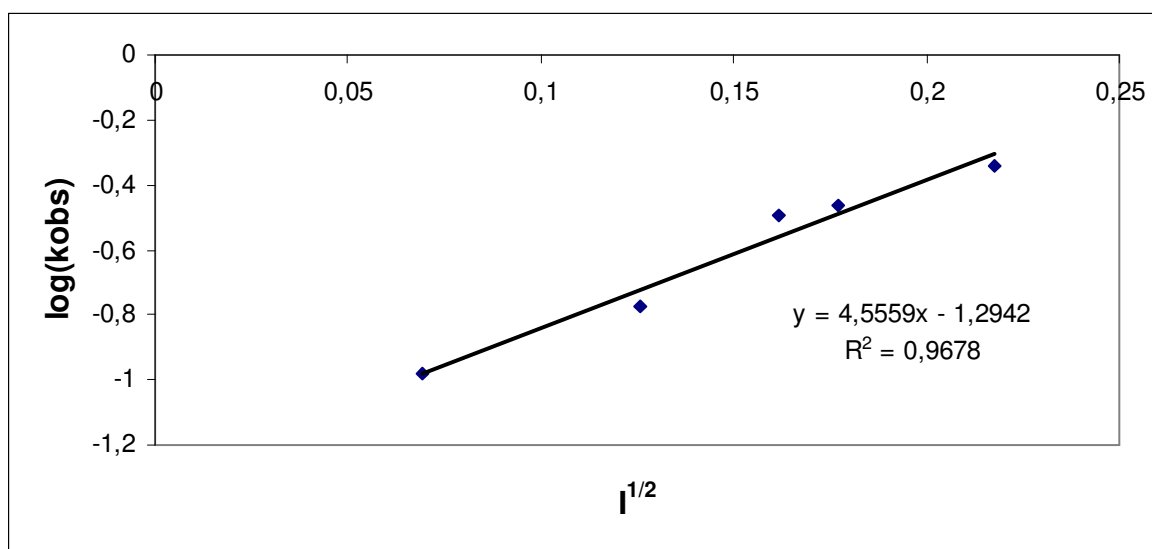
The nearly 5-fold change in the rate of decay of **1** and positive slope of 4.6 supports two similarly charged species interacting in the rate limiting step.

2.3. UV-Vis Kinetic Studies on Cu^{II} / H33m / TEMPO reaction

Under anaerobic and anhydrous conditions, CH$_3$CN solutions of TEMPO were added to the ligand in CH$_3$CN at 233 K, followed by Cu^{II}. The 425 nm band, which is assigned to species **1**, decays by a single exponential under conditions of excess TEMPO. Blank experiments with TEMPO and Cu^{II} and TEMPO and ligand discarded any interference at the 425 wavelength.

Dependence of k_{obs} on [TEMPO] (T = 233 K)

a) [Cu]= 1.25 mM, [H33m]= 1.25 mM, [TEMPO]= 5.0 mM
b) [Cu]= 1.25 mM, [H33m]= 1.25 mM, [TEMPO]= 7.5 mM
c) [Cu]= 1.25 mM, [H33m]= 1.25 mM, [TEMPO]= 10.0 mM

[TEMPO] (mM)	k_{obs} (min^{-1})
5	1.16
7.5	1.81
10	2.4
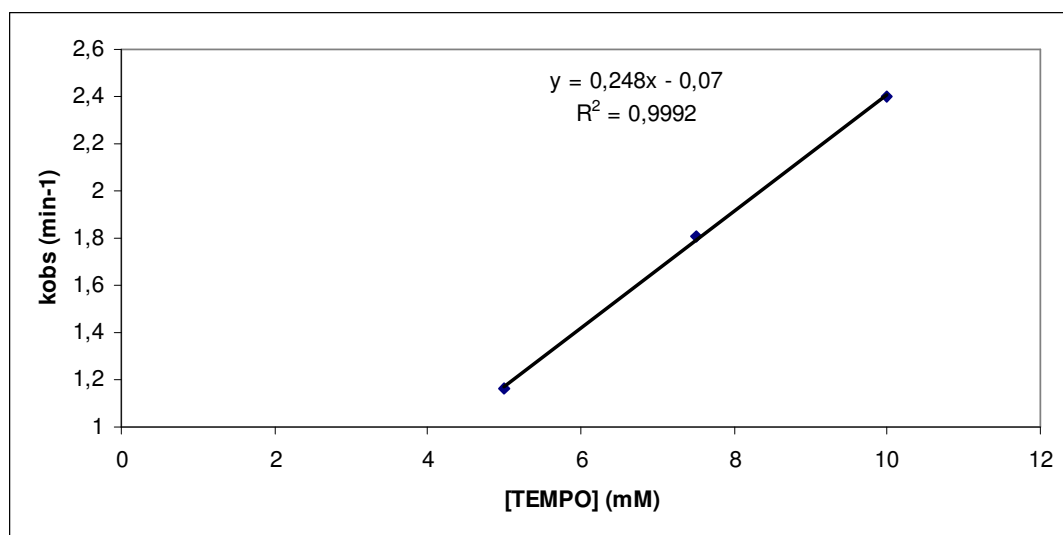
k_{obs} is linearly dependent on [TEMPO].

A [H33m] to [D-H33m] k_H/k_D kinetic isotope effect of 3.0 was measured with a 1.3:1.0:4.0 ligand:$Cu^{II}(CF_3SO_3)_2$:TEMPO initial conditions ($[Cu^{II}(CF_3SO_3)_2]$ = 1.25 mM, [Ligand] = 1.625 mM, [TEMPO] = 5,0 mM, 233 K, CH_3CN, N_2 atmosphere, Ligand = H33m or D-H33m); Figure S6.

k_{obs} dependence of Ionic strength (T = 233 K)

a) [Cu]= 1.25 mM, [H33m]= 1.625 mM, [TEMPO]= 5mM, [NaBARF]=0 mM
b) [Cu]= 1.25 mM, [H33m]= 1.625 mM, [TEMPO]= 5mM, [NaBARF]=4.17 mM
c) [Cu]= 1.25 mM, [H33m]= 1.625 mM, [TEMPO]= 5mM, [NaBARF]=8.3 mM

[NaBARF] (mM)	$I^{1/2}$	k_{obs} (s^{-1})	log(k_{obs})
0	0.069249	0.007867	-2.104171
4.17	0.100637	0.007697	-2.113700
8.3	0.124134	0.008771	-2.056937
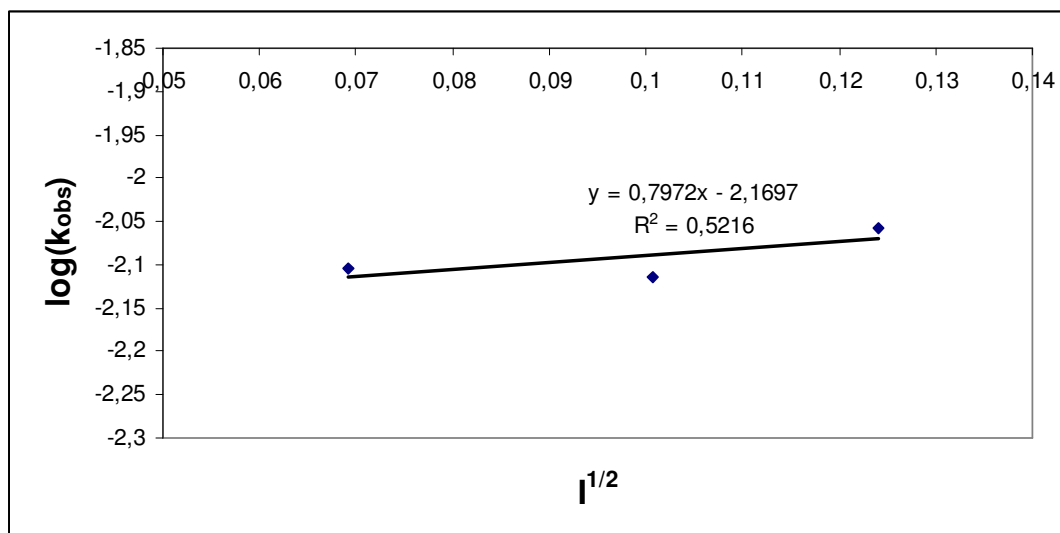
The k_{obs} values are not appreciably changed with a change in the ionic strength. The first-order dependence insensitivity is consistent with a neutral species involved in the rate limiting step, i.e. TEMPO.

Activation parameters of Cu^{II} / H33m / TEMPO reaction

The activation parameters have been obtained by means of Eyring analysis in the 233-263 K temperature range. The values of k_{obs} were determined at different temperatures and fitted to the Eyring to obtain the activation parameters $\Delta H^{\ddagger}$ and $\Delta S^{\ddagger}$:

$$\ln(k/T) = 23.76 + \Delta S^{\ddagger}/R - \Delta H^{\ddagger}/RT$$

The experimental conditions have been the following: [Cu]= 1.25 mM, [H33m]= 1.625 mM, [TEMPO]= 5 mM, CH_3CN, N_2 atmosphere.

T (K)	k_{obs} (s^{-1})	1/T	k_{obs}/T	ln(k_{obs}/T)
263	0.14828	0.00380	0.00056	-7.48081
253	0.05471	0.00395	0.00022	-8.43913
243	0.02527	0.00412	0.00010	-9.17113
233	0.00829	0.00429	0,00004	-10.24358
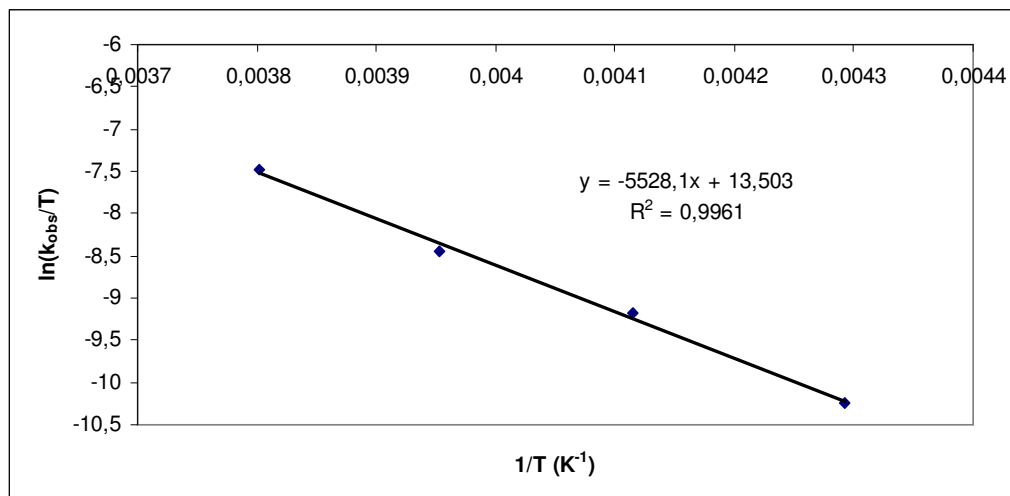
The values obtained are $\Delta H^{\ddagger}$ = 11.0 ± 0.5 kcal mol^{-1}, $\Delta S^{\ddagger}$ = -20.4 ± 2.0 cal K^{-1} mol^{-1}.

The enhanced decay species **1** with TEMPO is visualized by first formation of **1** under the condition of excess copper at 298 K, followed by addition of 1 equivalent of TEMPO (Figure S6d).

These experimental evidences are consistent with a PCET ratelimiting step for the aromatic C-H bond activation reported here. Recently, Yu and coworkers reported a catalytic Cu^{II}-mediated oxidative functionalization of arene C-H bonds at elevated temperatures.[24] With no appreciable kinetic isotope effect for C-H activation, a rate-limiting single electron transfer (SET) from the arene ring pyridyl ligated Cu^{II} ion was proposed, yielding an arene-radical-cation coupled to Cu^{I}. This proposal is consistent with the slower reactivity of more electron-deficient arenes. In the case of the C-H activation reported here, the appreciable kinetic isotope effect of 2.6 at 286 K and the faster reactivity of the more electron-deficient pNO$_2$-H33m ligand (Figure S10) suggest a different mechanism is operative.

2.4. UV-Vis and ^{1}H-NMR Kinetic Studies on Ni^{II} / H33m reaction

Systematic kinetic studies to determine the reaction rate dependence on [Ni^{II}] and [H33m] were performed under anaerobic and anhydrous conditions in CH_3CN. The 400 nm feature that forms upon mixing the H33m and Ni^{II} corresponds to product **4**. The formation follows a single exponential profile (Figure S7), and k_{obs} is unaffected by excess H33m or Ni^{II}. H33m and Ni^{II}(ClO$_4$)$_2$·6H$_2$O were mixed in a 1.3:1 molar ratio ([Ni^{II}] = 2.2 mM) in d$_3$-acetonitrile. The initially formed species was characterized at 248 K by ^{1}H-NMR (Figure S8), and the reaction was followed at 298 K by the appearance of the resonances corresponding to [Ni^{II}(H33m-C)](ClO$_4$) (**4**·(ClO$_4$)). The single exponential fit to the data gives a k_{obs} = 2.9 x 10^{-4} s^{-1} (Figure S9), a rate very similar to that measured by UV-Vis analysis of the reaction at 300 K (k_{obs} = 5.5 x 10^{-4} s^{-1}). Full assignment of ^{1}H and ^{13}C signals of **4** was achieved through COSY and HSQC ^{1}H-^{13}C correlations.

3. SUPPLEMENTARY FIGURES

Figure S1. Experimental frozen-solution X-band cw EPR spectra at 120 K of (A) $Cu^{II}(CF_3SO_3)_2$ and (B) **1**•$(CF_3SO_3)_2$ in butyronitrile, initially formed at 253 K. Spectrum C is a simulation of B in which two copper species, spectra D and E, contribute in a 3:1 ratio, respectively.
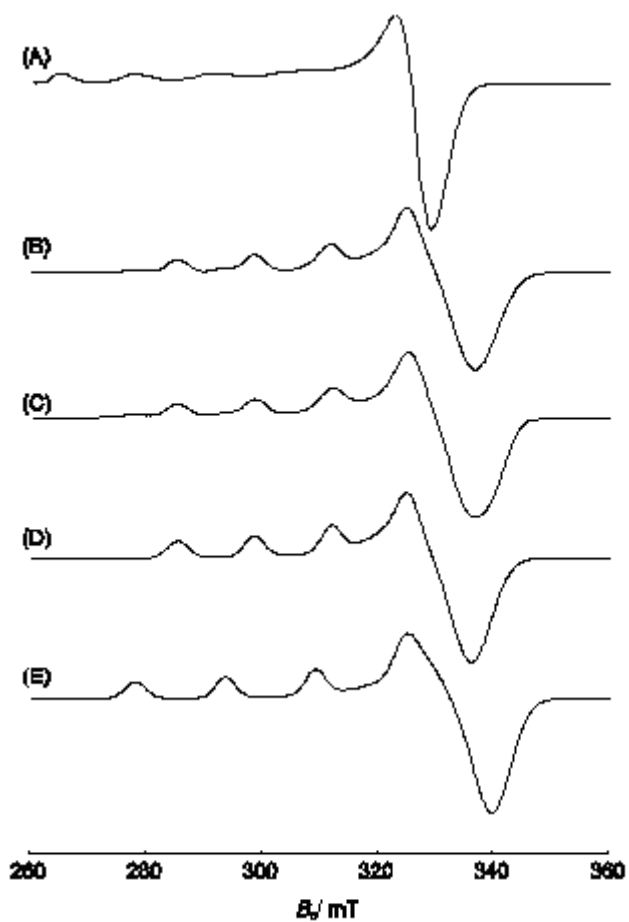
Figure S2. Experimental X-band Davies-ENDOR spectra of **1**•$(CF_3SO_3)_2$ (15 K). Black traces: spectra obtained using non-selective microwave (mw) pulses; gray traces: using selective mw pulses. Positions (A) and (B) in the inset indicate the observer positions and correspond to the shown HYSCORE observer positions (see Figure 3, main text). The position of the ^1H Larmor frequency is indicated as a dashed line.
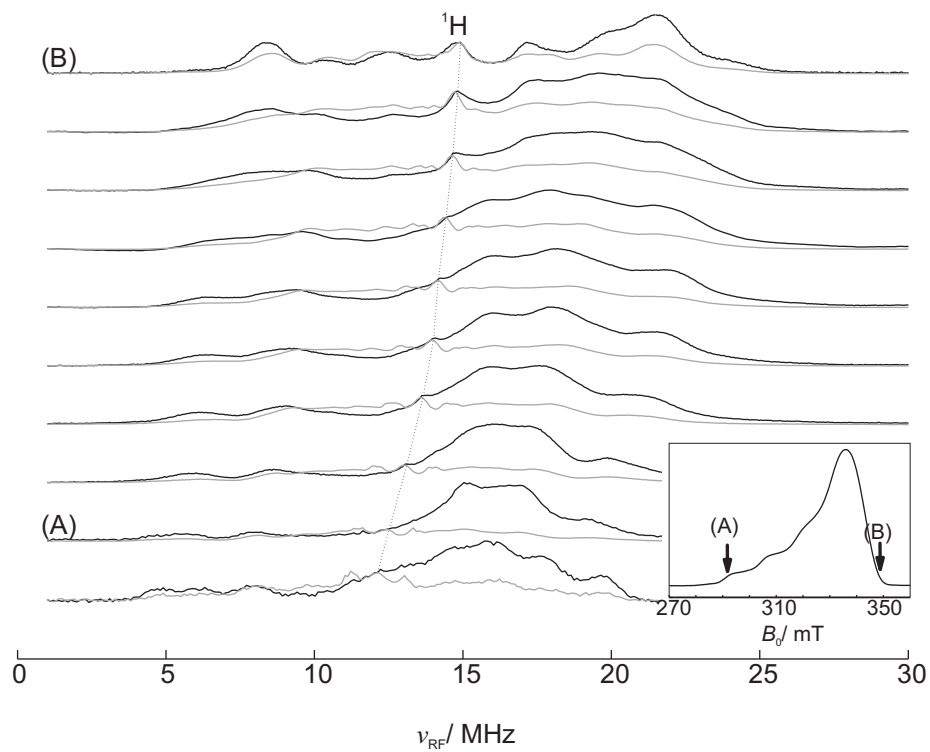
Figure S3. Experimental X-band cw EPR spectra at 120 K of (A) [Cu^{II}(D-H33m)](CF$_3$SO$_3$)$_2$ in butyronitrile (initially generated at 253 K) and (B) its simulation.
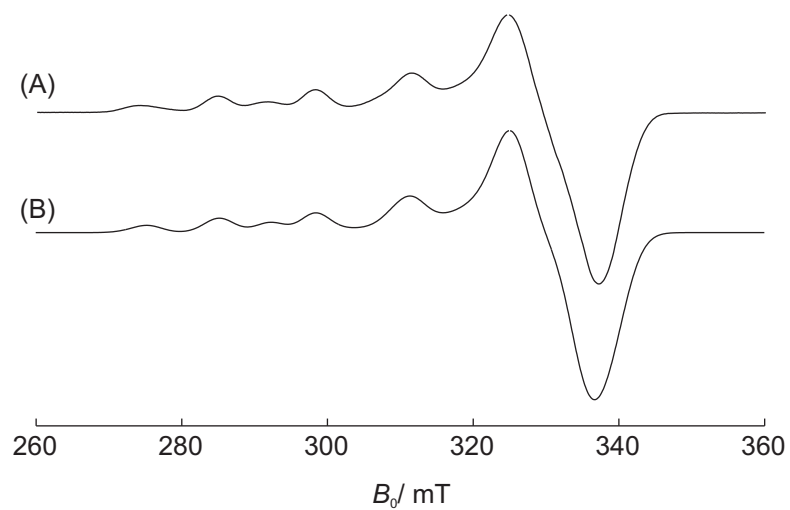
Figure S4. Experimental X-band Davies-ENDOR spectrum of [Cu^{II}(D-H33m)](CF$_3$SO$_3$)$_2$ recorded at the maximum echo position indicated by a bold arrow in the inset showing the corresponding FID-detected EPR spectrum (15 K). The ENDOR spectrum was recorded using selective pulses.
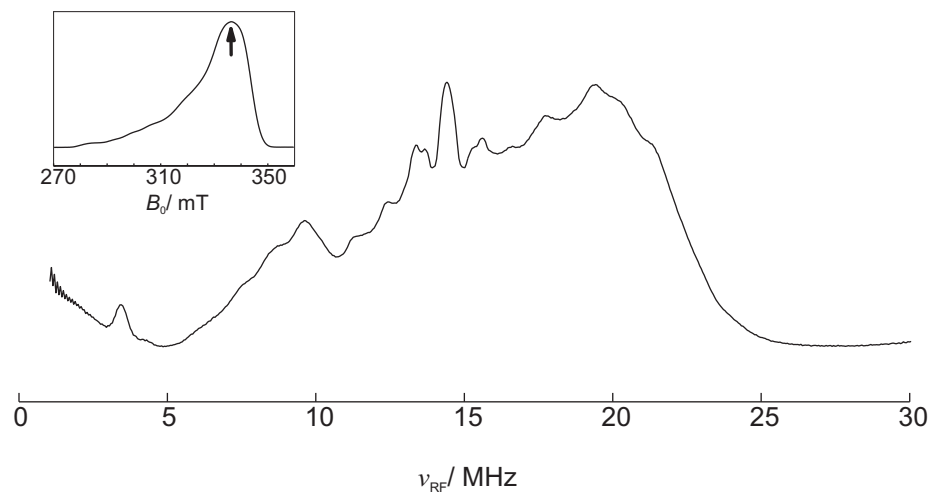
Figure S5. UV-Vis optical changes for the C-H$_a$ bond cleavage reaction of (a) 1.3:1.0 H33m:Cu^{II}(CF$_3$SO$_3$)$_2$ ([Cu^{II}(CF$_3$SO$_3$)$_2$] = 1.25 mM, [H33m] = 1.625 mM, 298 K, CH$_3$CN, N$_2$ atmosphere) (under these conditions, the reaction needed to be monitored at a single wavelength (425 nm)) and (b) 1.0:2.0 H33m:Cu^{II}(CF$_3$SO$_3$)$_2$ ([Cu^{II}(CF$_3$SO$_3$)$_2$] = 2.5 mM, [H33m] = 1.25 mM, 298 K, CH$_3$CN, N$_2$ atmosphere). Inset provides the decay profiles at 425 nm.

(a)
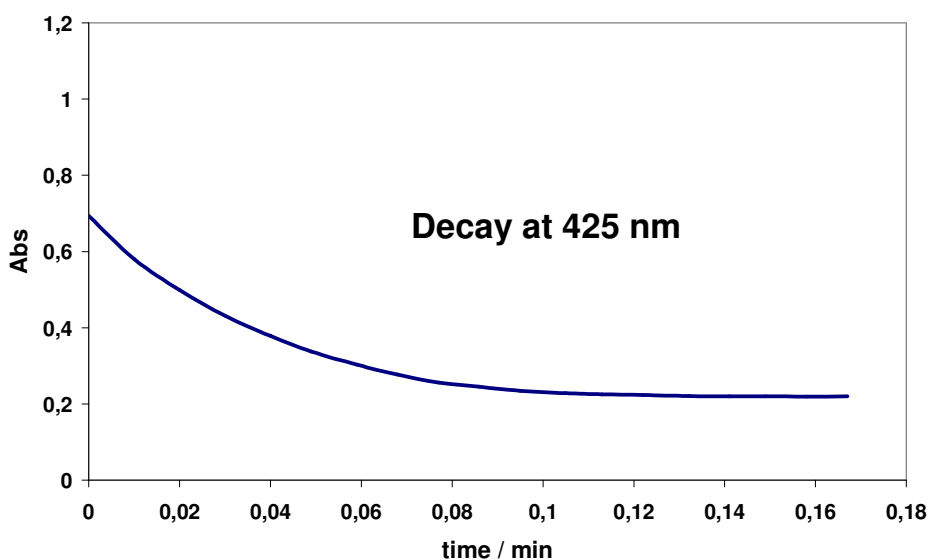
(b)
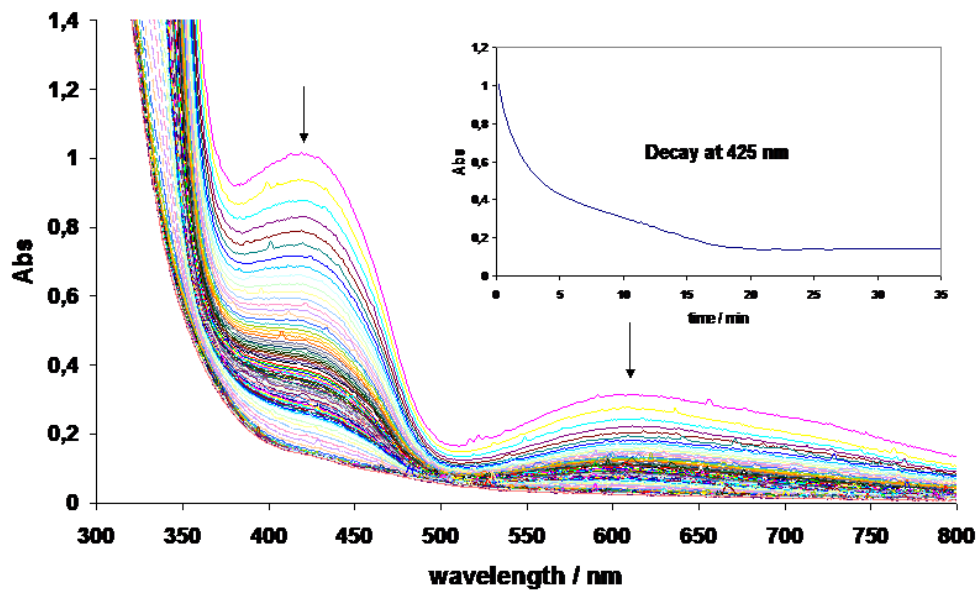
Figure S6. UV-Vis optical changes for the C-H$_a$ bond cleavage reaction of (a) 1.3:1.0:4.0 H33m:Cu^{II}(CF$_3$SO$_3$)$_2$:TEMPO ([Cu^{II}(CF$_3$SO$_3$)$_2$] = 1.25 mM, [H33m] = 1.625 mM, [TEMPO] = 5.0 mM, 233 K, CH$_3$CN, N$_2$ atmosphere), and (b) 1.3:1.0:4.0 D-H33m:Cu^{II}(CF$_3$SO$_3$)$_2$:TEMPO ([Cu^{II}(CF$_3$SO$_3$)$_2$] = 1.25 mM, [D-H33m] = 1.625 mM, [TEMPO] = 5.0 mM, 233 K, CH$_3$CN, N$_2$ atmosphere). Insets in (a) and (b) provide the decay profile at 425 nm, and the single exponential fit. (c) ^{1}H-NMR spectrum of the final solution (upon solvent evaporation and addition of CD$_3$CN; only Cu^{III}-Aryl product (**2**) and TEMPOH signals are observed). (d) ESI-MS of the same final solution. (e) Rapid decay of UV-Vis bands assigned to **1** upon addition of 1 equiv. of TEMPO ([Cu^{II}(CF$_3$SO$_3$)$_2$] = 1.625 mM, [H33m] = 1.25 mM, [TEMPO] = 1.25 mM, 298 K, CH$_3$CN, N$_2$ atmosphere). (f) No modification of the absorbance at 425 nm upon addition of 1 equiv. of ferrocenium cation ([Cu^{II}(CF$_3$SO$_3$)$_2$] = 1.25 mM, [H33m] = 1.25 mM, [Fc$^+$] = 1.25 mM, 233 K, CH$_3$CN, N$_2$ atmosphere). (g) Decay of 425 nm band for reaction of **1** with TEMPO upon addition of water ([Cu^{II}(CF$_3$SO$_3$)$_2$] = 1.25 mM, [H33m] = 1.625 mM, [TEMPO] = 5.0 mM, 233 K, N$_2$ atmosphere, CH$_3$CN/H$_2$O (final volume = 3 mL, additions of 0.0 µL (k_{obs}=0.012 ± 2·10^{-5} s^{-1}), 2.5 µL (k_{obs}=0.017 ± 2·10^{-5} s^{-1}) and 5.0 µL (k_{obs}=0.030 ± 4·10^{-5} s^{-1}) of H$_2$O)).

(a)

(b)

(c)

1HRMN [CuII]=[H33m]=1.25mM
[TEMPO-rad] = 3.75mM

(d)

Acquisition Parameter
Ion Source Type   ESI   Ion Polarity   Positive   Alternating Ion Polarity   off
Mass Range Mode   Std/Enhanced   Scan Begin   100 m/z   Scan End   600 m/z
Capillary Exit   121.0 Volt   Skimmer   40.0 Volt   Trap Drive   41.4
Accumulation Time 3842 µs   Averages   7 Spectra   Auto MS/MS   off

$[(aryl\text{-}Cu^{III})(OTf)]^+$
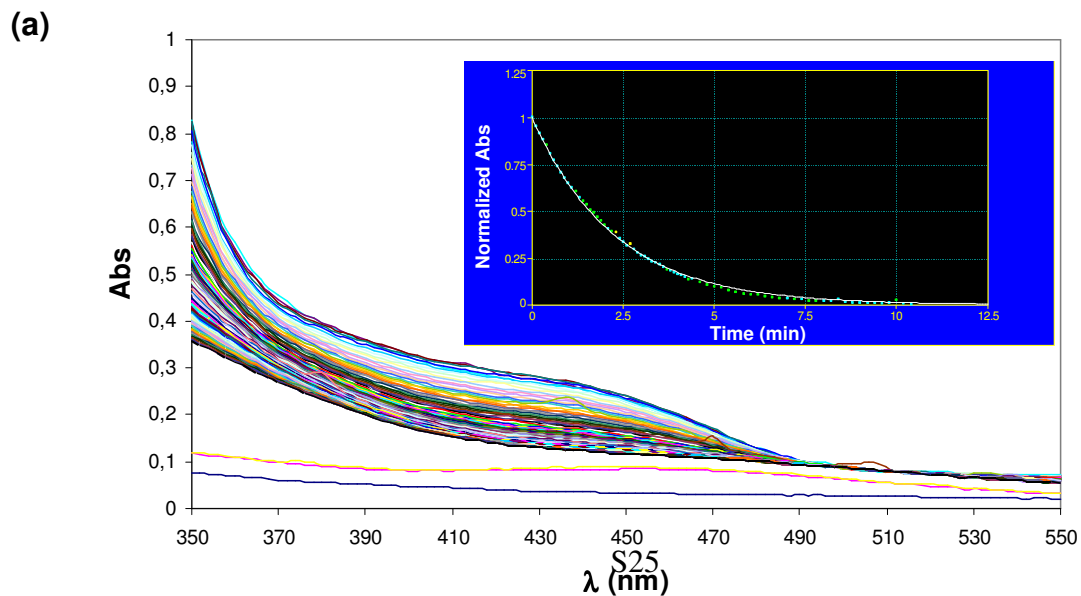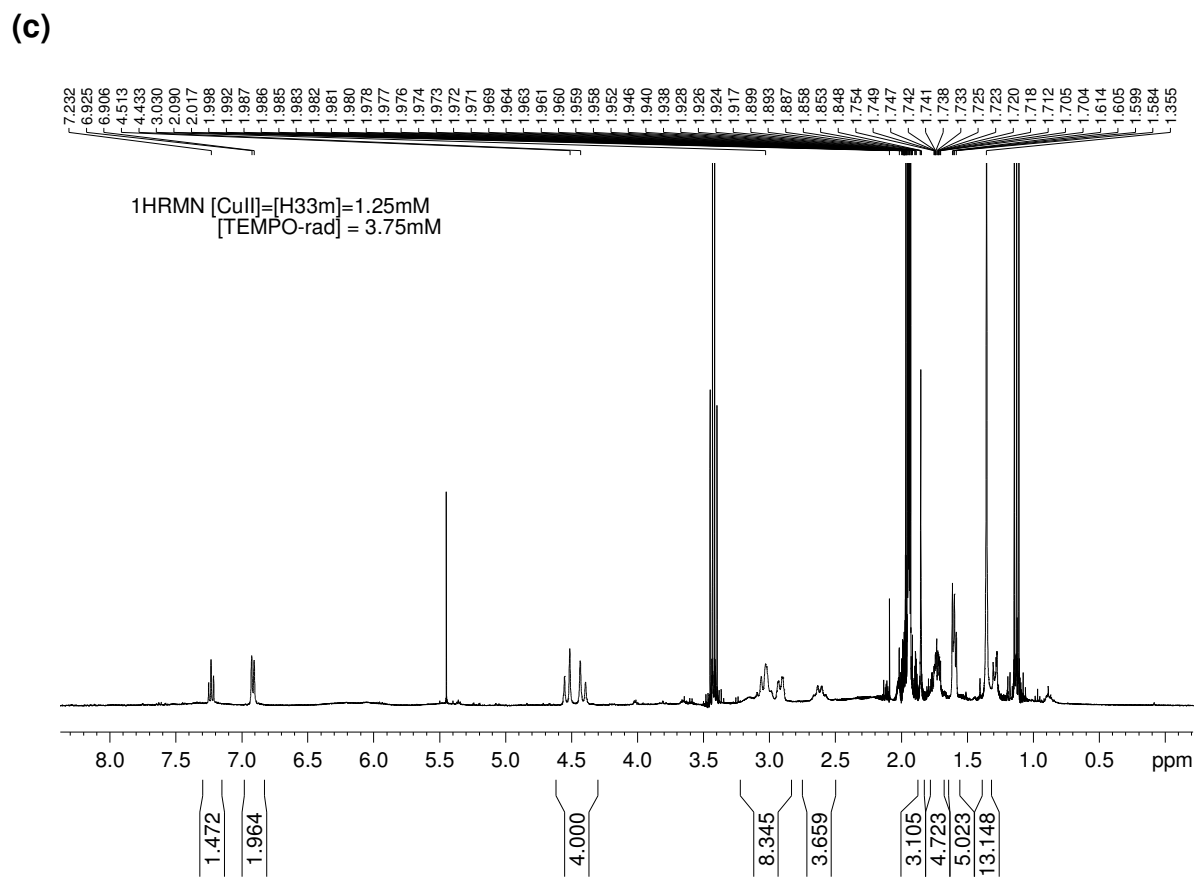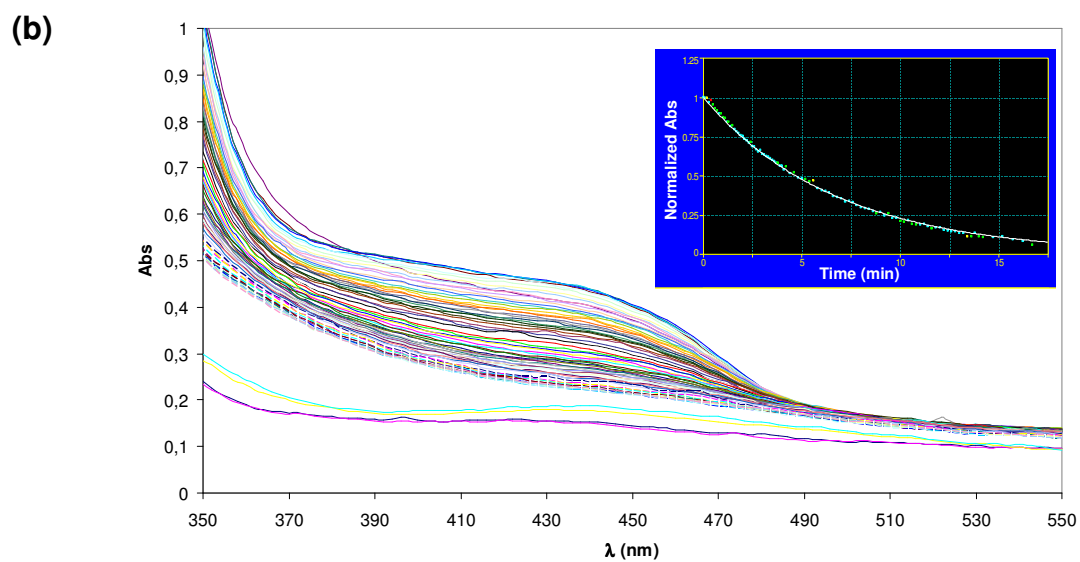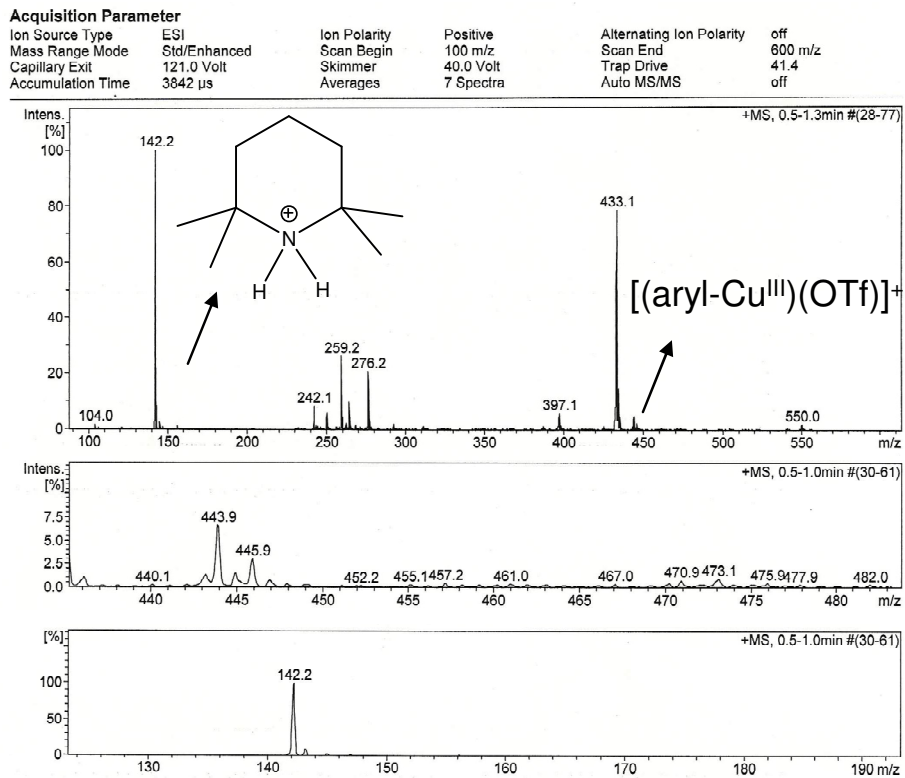
(e)
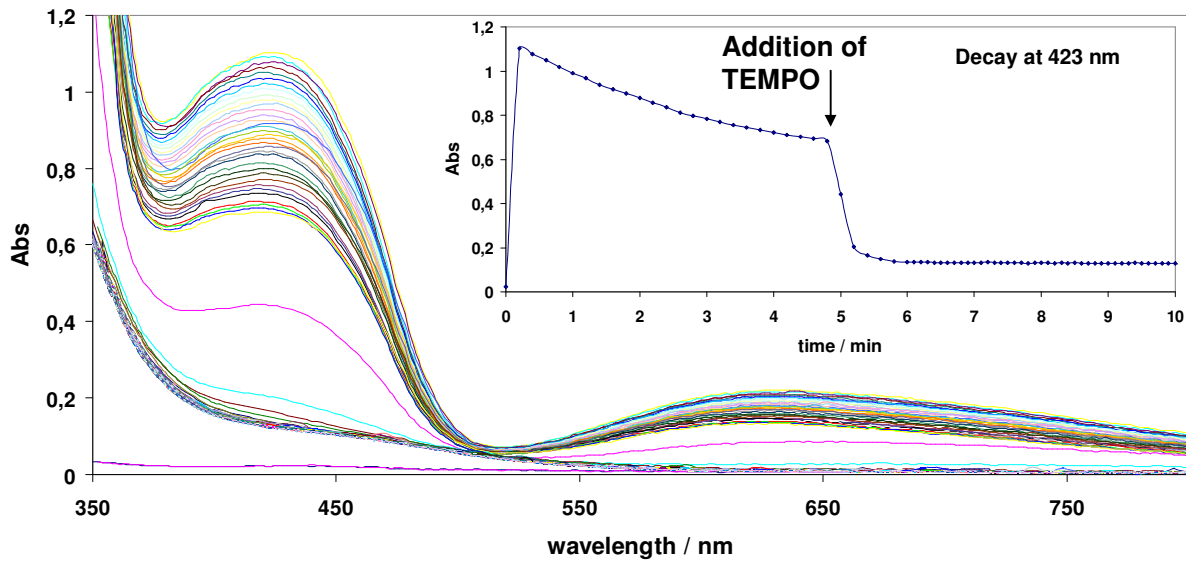
(f)
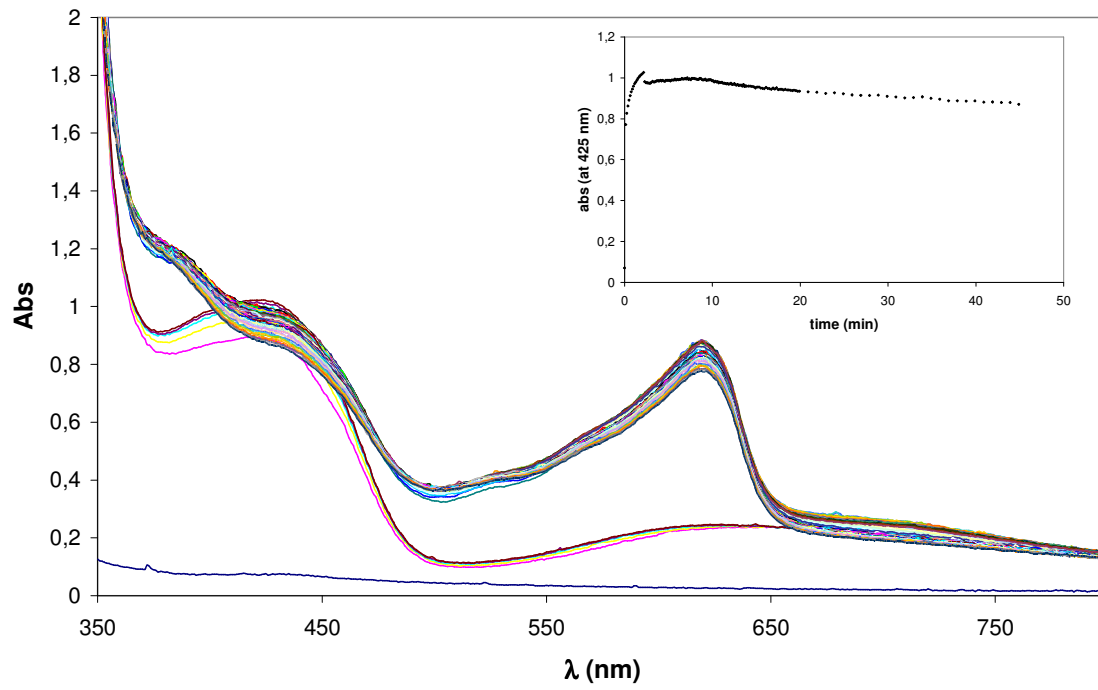
(g)
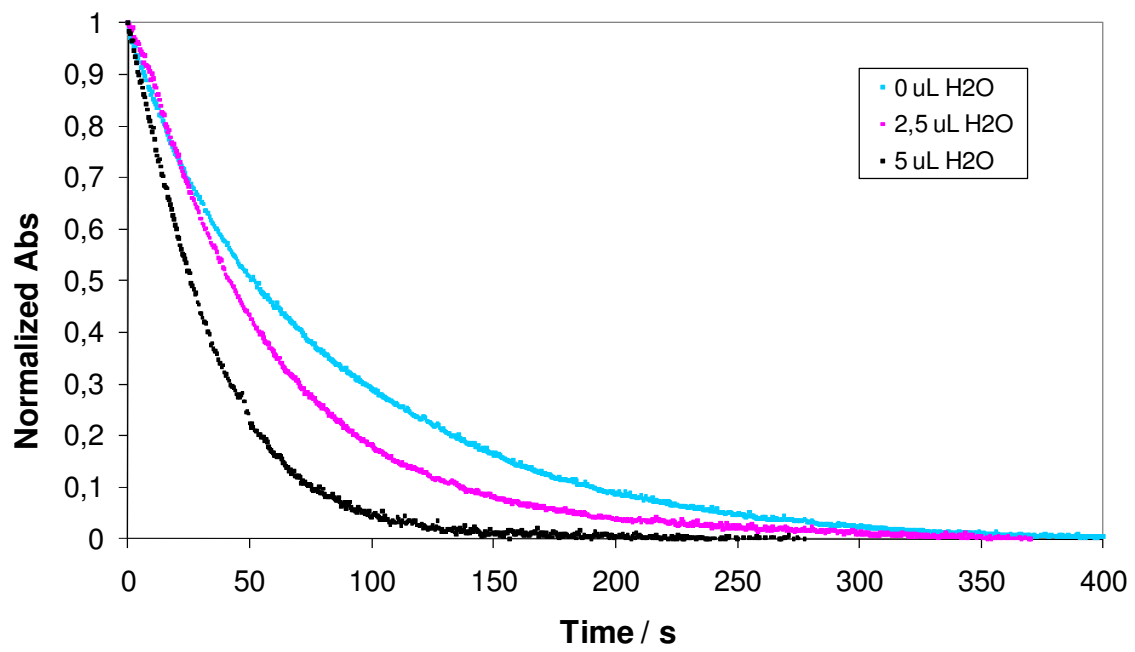
Figure S7. UV-Vis optical changes associated with (a) the C-H$_a$ bond activation using a 1.3:1 H33m:Ni^{II} molar ratio ([Ni^{II}] = 2.5 mM, 286 K, CH$_3$CN, N$_2$ atmosphere) and (b) the 400 nm band (corresponding to **4**) growing profile under increasing [H33m] ([Ni^{II}] = 1.25 mM, 298 K, CH$_3$CN, N$_2$ atmosphere).

(a)
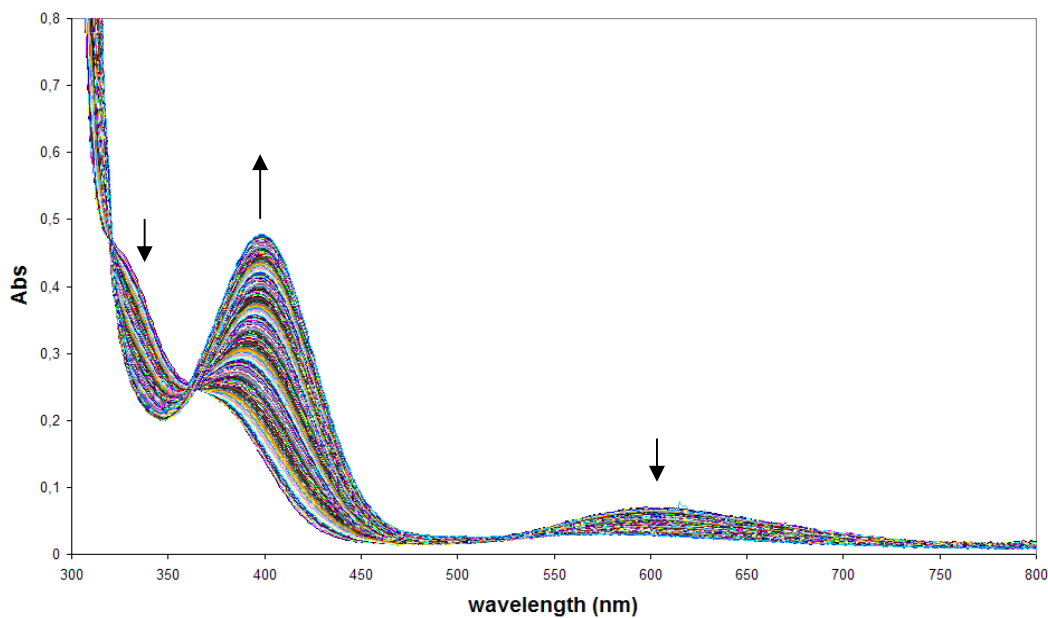
(b)
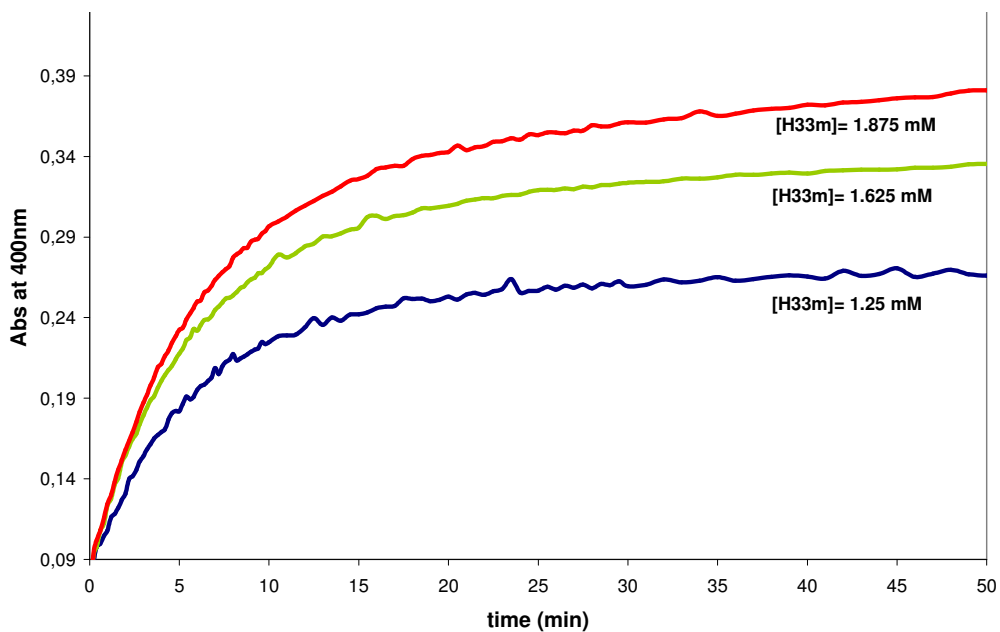
Figure S8. ^{1}H-NMR spectra of the paramagnetic species [Ni^{II}(H33m)(CH$_3$CN)]$^{2+}$ (**3**) and the corresponding mono-deuterated analogue (248 K, -50 to 1000 ppm measured, -30 to 500 ppm window shown). Arrows indicate the H$_a$ signal corresponding to free ligand H33m in solution, and its absence for D-H33m system.
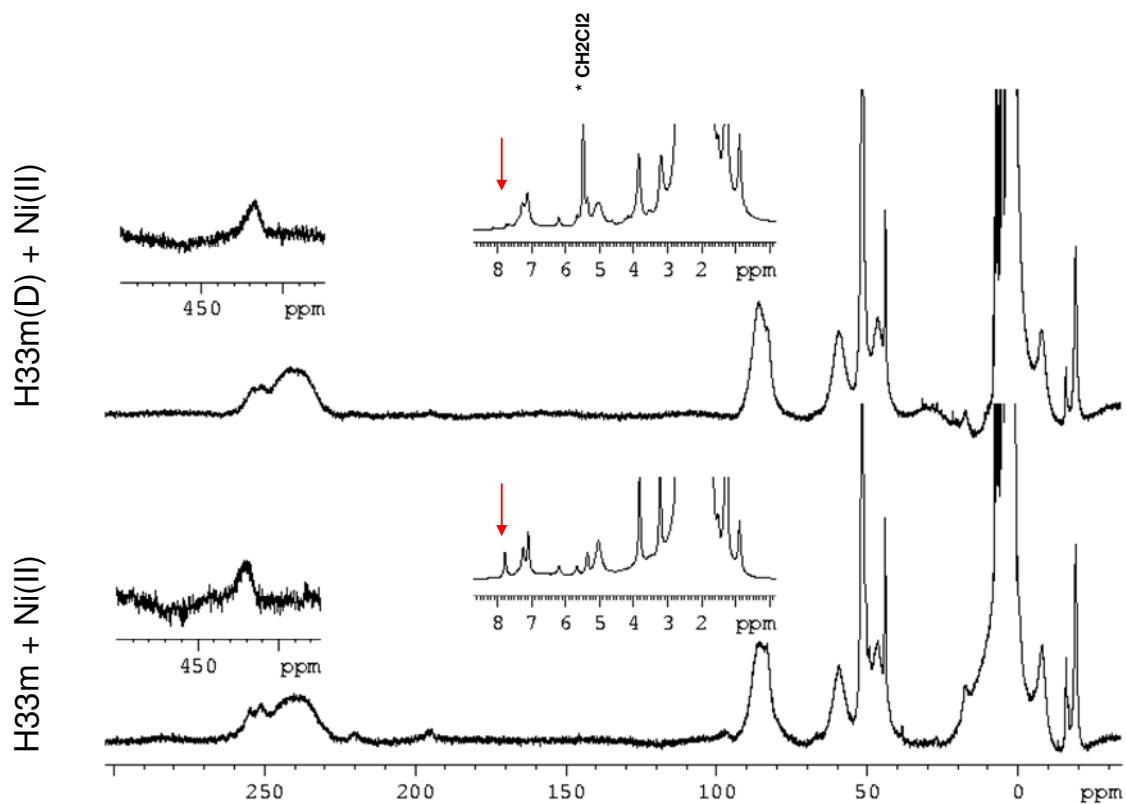
Figure S9. ^{1}H NMR kinetic monitoring of the reaction of H33m and Ni^{II}(ClO$_4$)$_2$·6H$_2$O (CD$_3$CN, 1.3:1 H33m:Ni^{II} molar ratio, [Ni^{II}] = 2.2 mM, 298 K). (a) ^{1}H-NMR spectra (range 6.6-8.2 ppm) at different times (spectrum of free ligand H33m, inset shows fitting to first-order kinetics, k_{obs} = 2.9 x 10^{-4} s^{-1}). (b) Full-range ^{1}H-NMR spectrum of the reaction mixture at 43 min after mixing. The peaks corresponding to **4** are marked with asterisks.

(a)
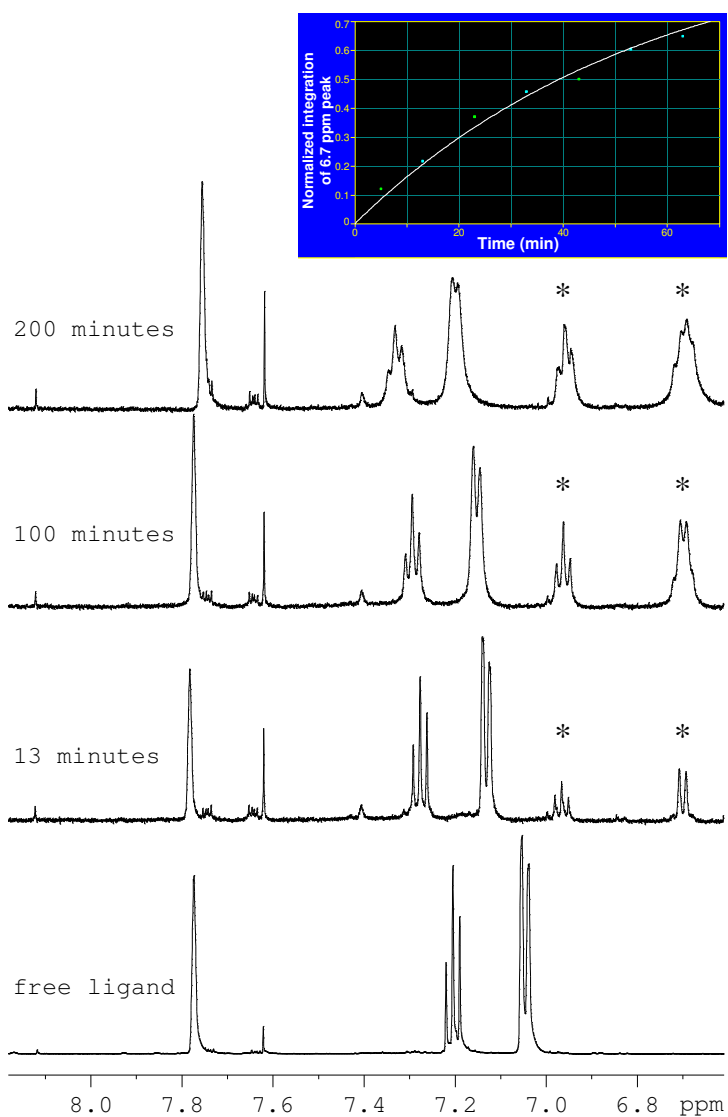
(b)
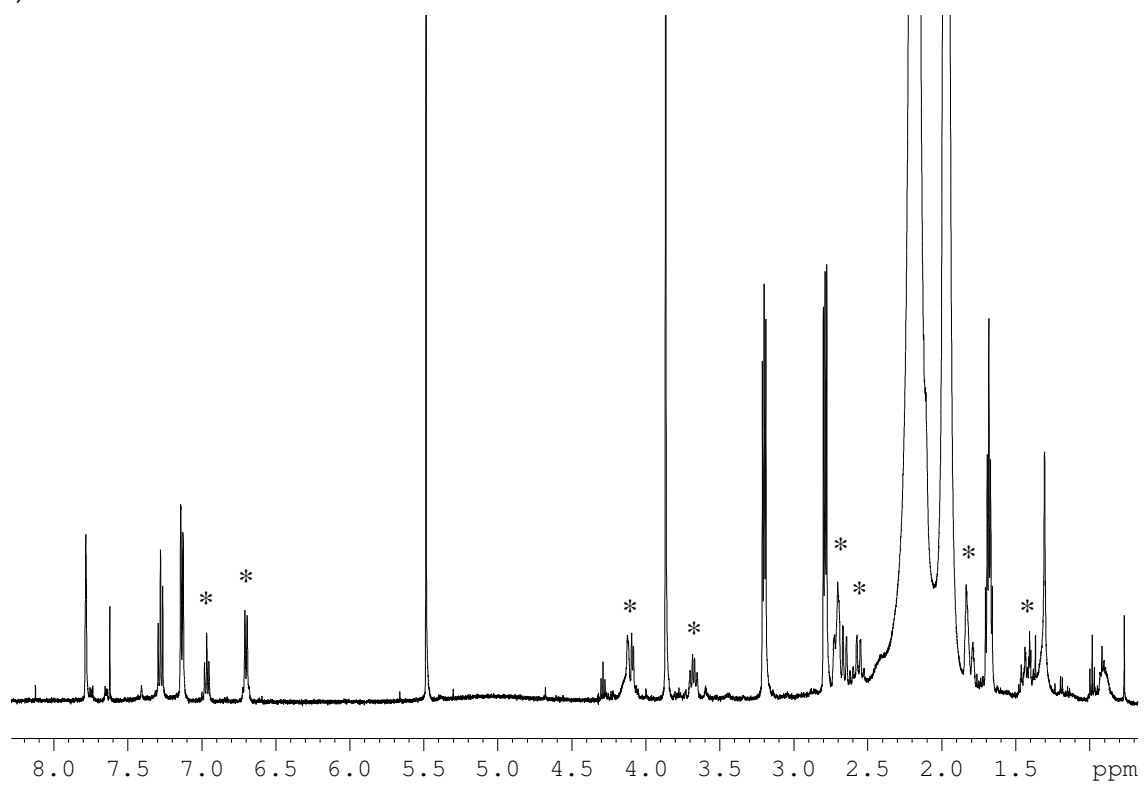
Fig. S10. UV-Vis absorption decay at 425 nm for the disproportionation reaction by [Cu^{II}(*p*-NO$_2$-H33m)]$^{2+}$ and [Cu^{II}(H33m)]$^{2+}$ under excess of copper ([H33m] = 1.25 mM, [Cu^{II}] = 1.875 mM, 298 K, CH$_3$CN, N$_2$ atmosphere).
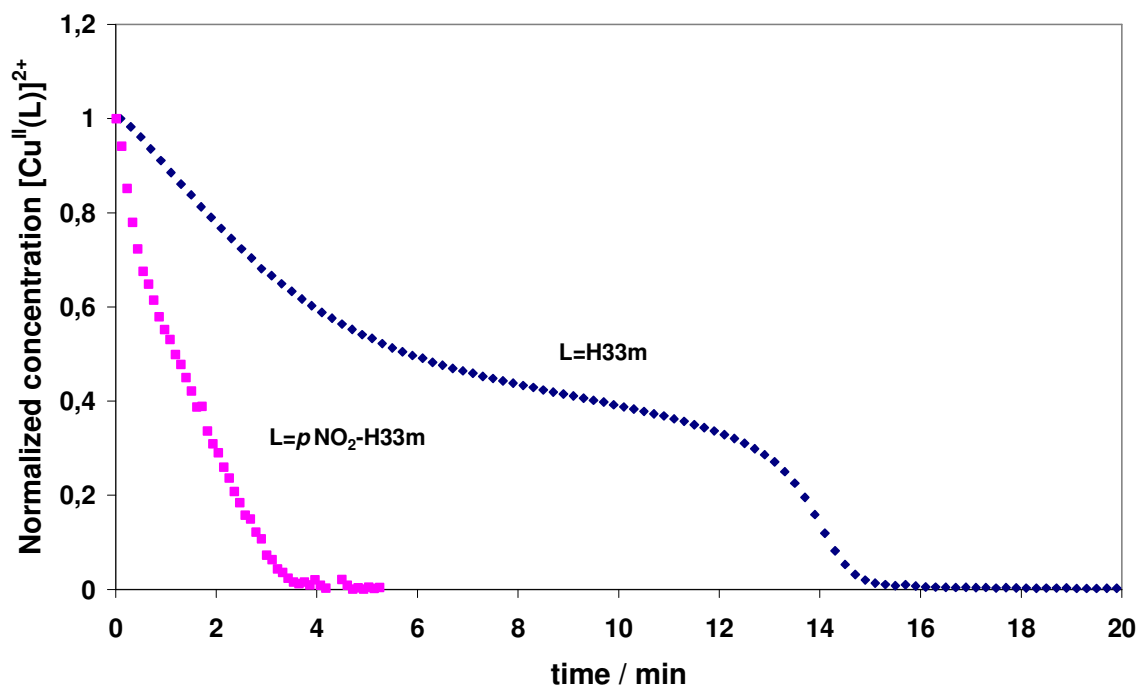
Fig. S11. Speciation profiles for Cu^{II}-containing species in the 5-step mechanistic model (see Figure 6c, main text) (A = Cu^{II}, C = **1**, D = [Cu^{II}L$_2$]$^{2+}$, E = [(Cu^{II})$_2$L]$^{4+}$). Cu^{II}-containing species with a significant concentration with respect to species C (complex **1**) correspond to experiments under excess-copper conditions: (a) [Cu^{II}]= 2 mM, [H33m]= 1.25 mM, (b) [Cu^{II}]= 1.875 mM, [H33m]=1.25mM, (c) [Cu^{II}]= 1.625 mM, [H33m]=1.25mM, (d) [Cu^{II}]= 1.435 mM, [H33m]=1.25mM .

(a)

(b)

(c)

[Cu]=1.625 mM, [H33m]=1.25 mM

(d)

[Cu]=1.435 mM, [H33m]=1.25 mM
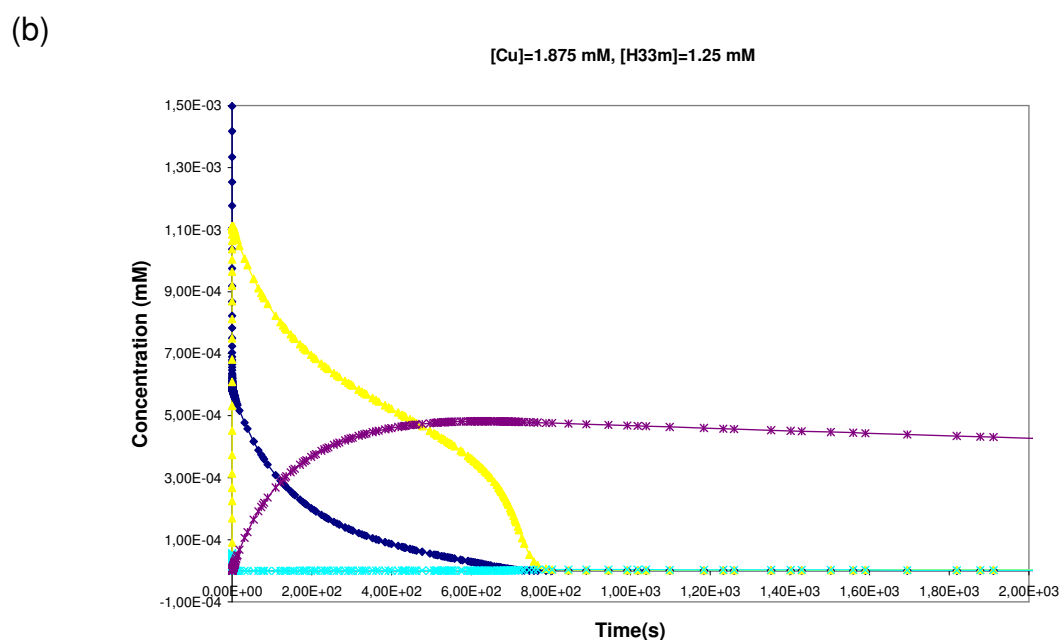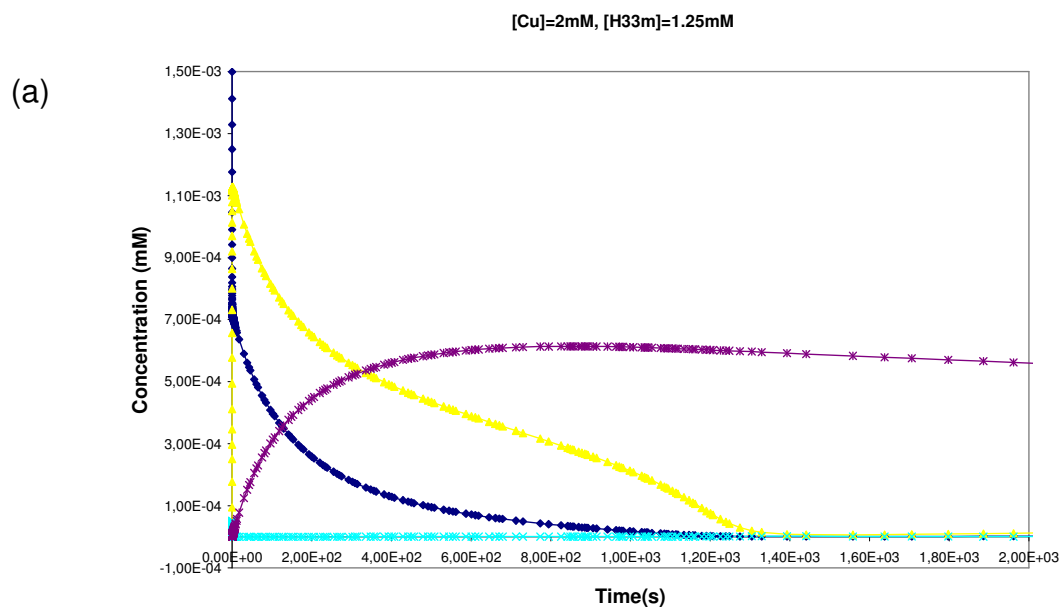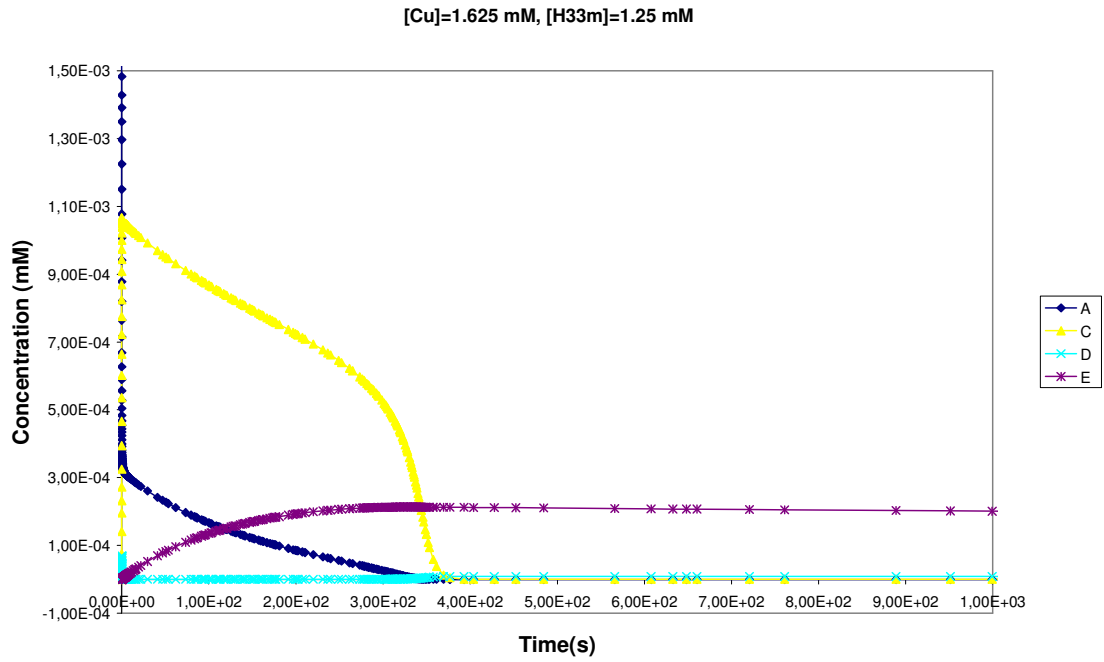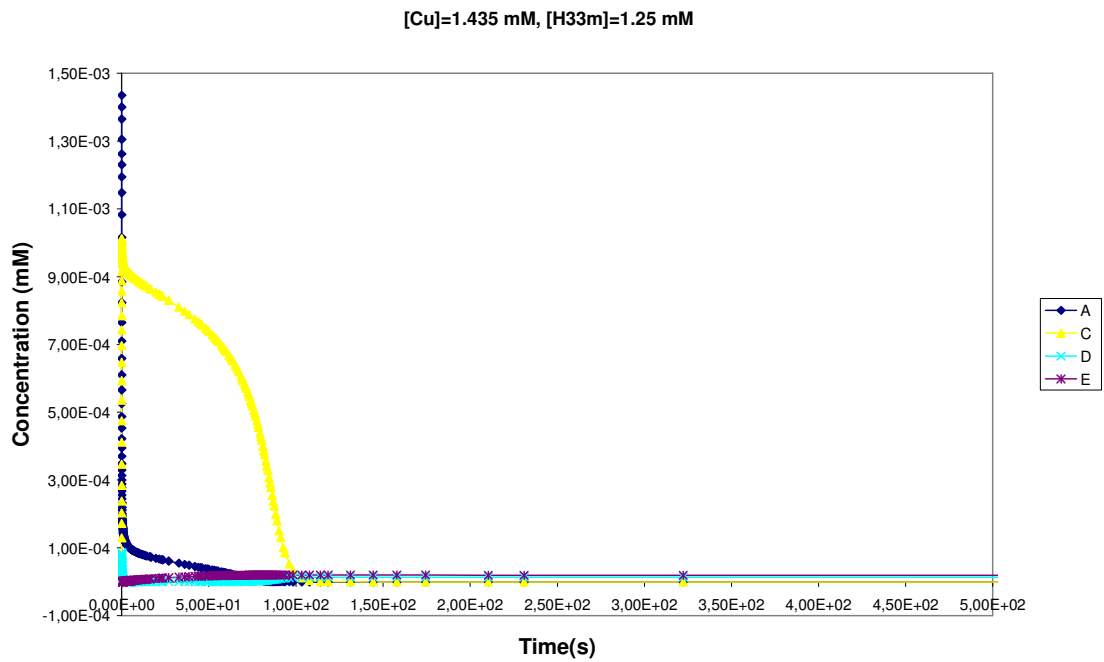
Fig. S12. Decay profiles at 425 nm of complex **1** under excess-ligand conditions ([H33m]=1.625mM, [Cu^{II}]= 1.25 mM) and addition of (a) distilled water (0.17% and 0.33% v/v) or (b) aqueous solution of KH$_2$PO$_4$/Na$_2$HPO$_4$ buffer (0.17% and 0.33% v/v of a 30 mM buffer solution (pH=7.14)).
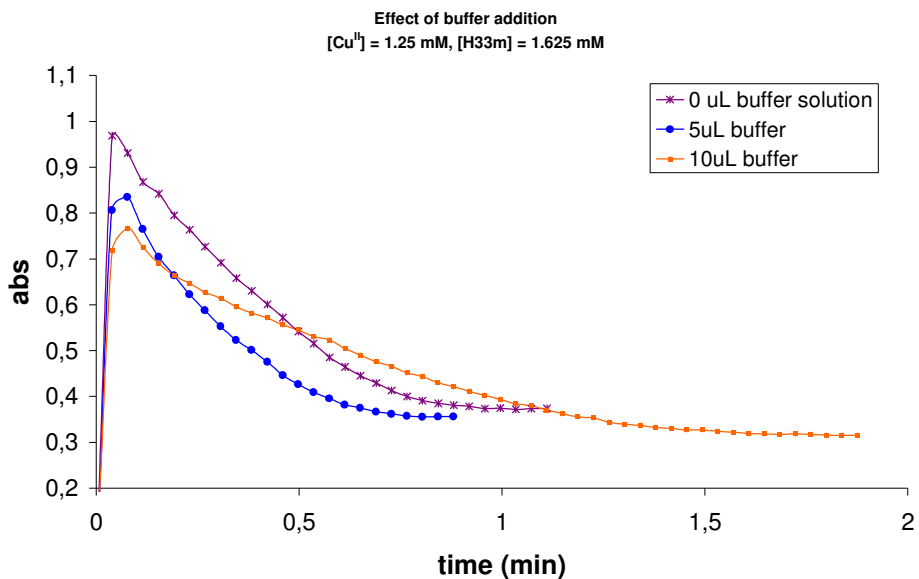
(a)
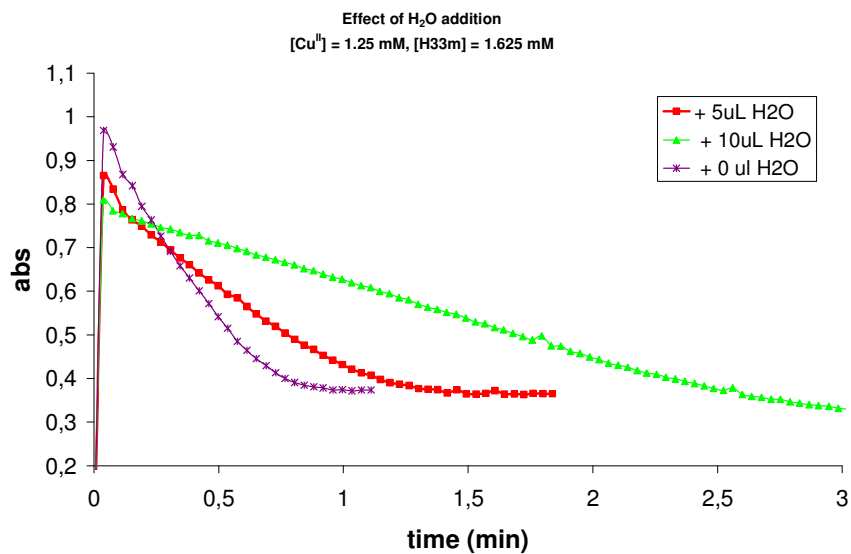
(b)

Fig. S13. Reaction of complex **1** with two equivalents of 1,10-phenanthroline caused a sharp decay of the 425 nm band towards unknown products. No sign of formation of complex $[Cu^I(phen)_2]^+$ is found thus excluding the presence of Cu^I before the disproportionation (this complex presents an absorption band at 436 nm (ε = 5400 $M^{-1}cm^{-1}$)). Experimental conditions: [H33m] = 1.625 mM, $[Cu^{II}]$ = 1.25 mM, [phen] = 2.5 mM, CH_3CN, N_2 atmosphere).
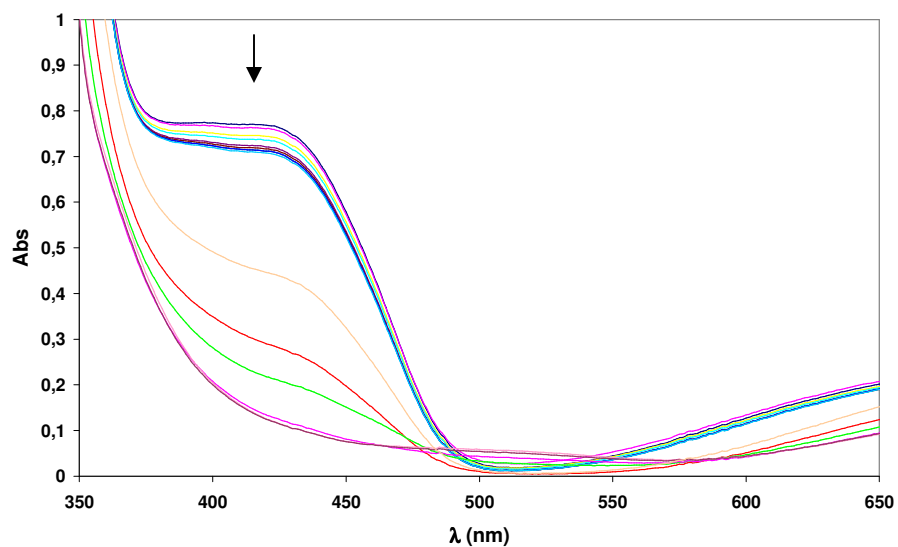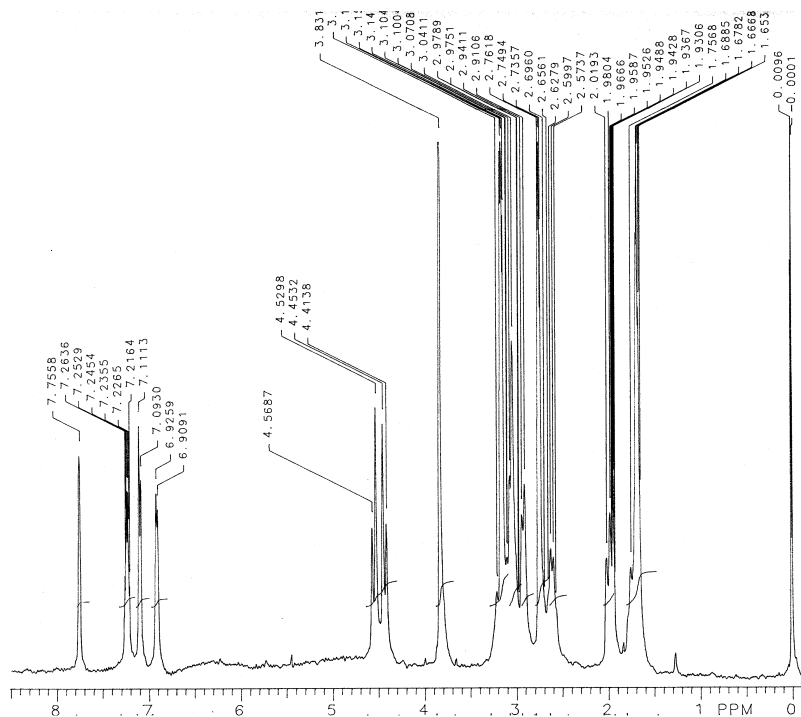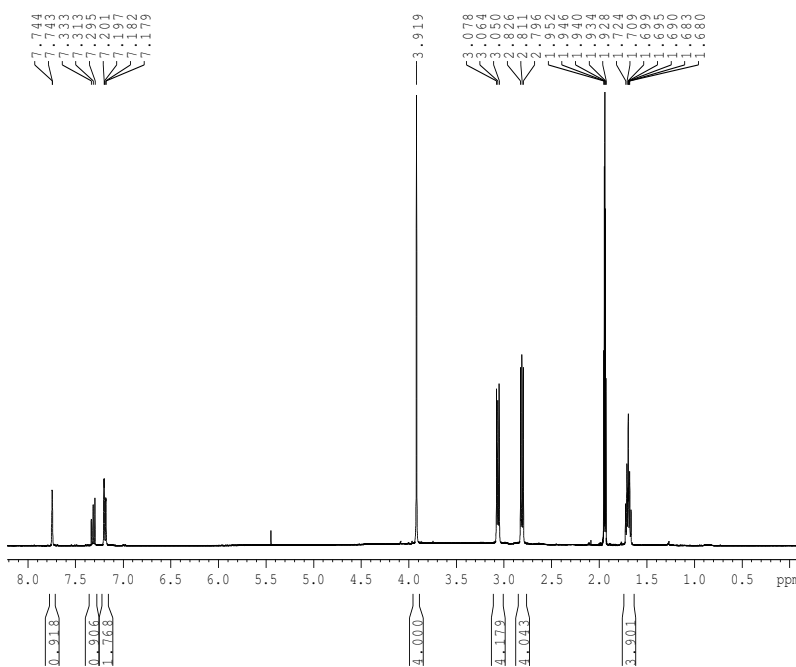
Fig. S14. Products of the disproportionation reaction of the H33m/Cu[II] system. (a) ^{1}H NMR (400 MHz, 298 K, CD$_3$CN) spectra for final disproportionation reaction mixture for [aryl-Cu[III]]$^{2+}$/[Cu[I](CH$_3$CN)$_4$]$^+$/[H33mH]$^+$. (b) ^{1}H NMR (400 MHz, 298 K, CD$_3$CN) of metal-free H33m ligand with 1 equiv. of CF$_3$SO$_3$H. (c) ESI-MS spectrum of the final disproportionation reaction mixture for [aryl-Cu[III]]$^{2+}$/[Cu[I](CH$_3$CN)$_4$]$^+$/[H33mH]$^+$.

(a)

(b)

(c)

Acquisition Parameter

Ion Source Type	ESI	Ion Polarity	Positive	Alternating Ion Polarity	off
Mass Range Mode	Std/Normal	Scan Begin	100 m/z	Scan End	1000 m/z
Capillary Exit	121.0 Volt	Skimmer	40.0 Volt	Trap Drive	41.3
Accumulation Time	1785 µs	Averages	7 Spectra	Auto MS/MS	off
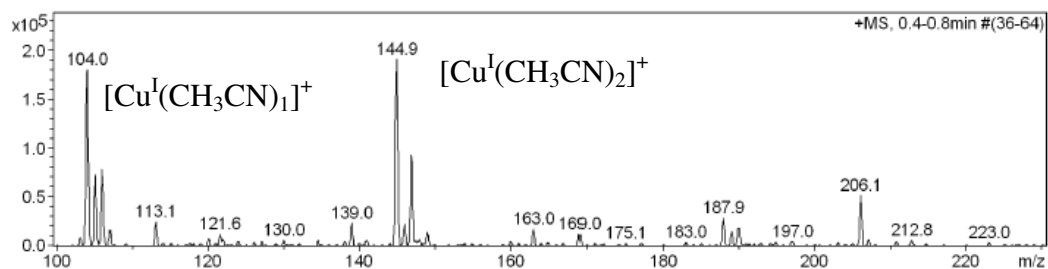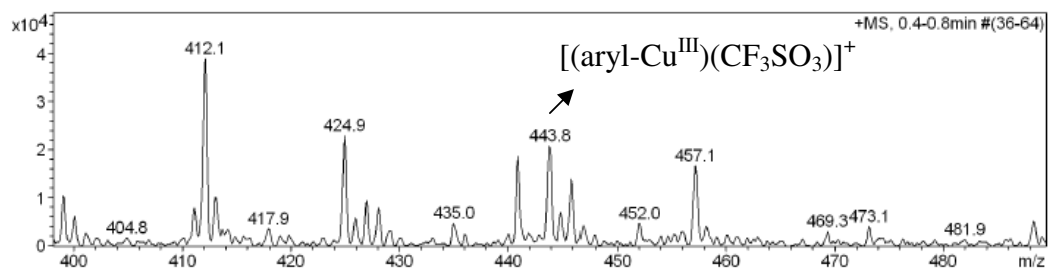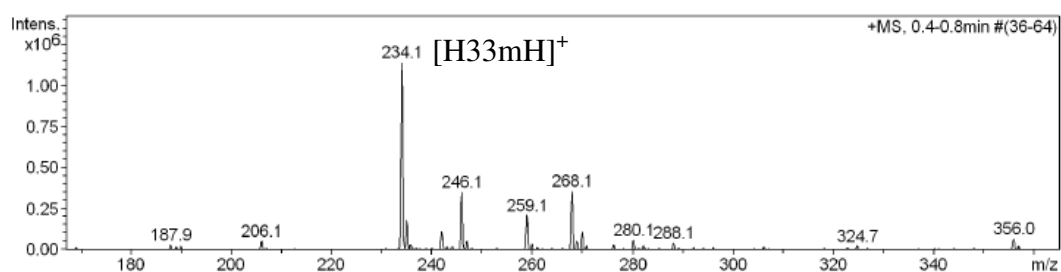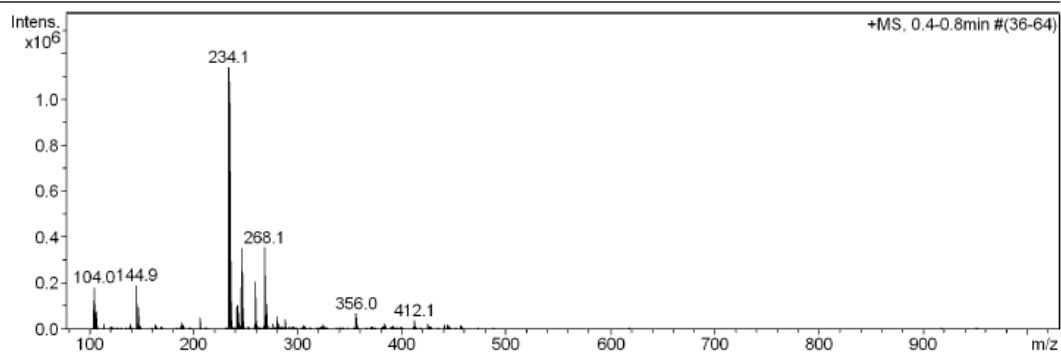
4. SUPPLEMENTARY TABLES

Table S1. Crystal structure details of complex [Ni^{II}-aryl](NO$_3$) (**4·(NO$_3$)**). CCDC deposit number 726565.

	Complex 4·(NO$_3$)
Empirical formula	C18.67 H29.33 N5.33 Ni1.33 O4
Formula weight	470.75
Temperature	153(2) K
Wavelength	0.71073 Å
Crystal system	Monoclinic
Space group	P2(1)/c
Unit cell dimensions	a = 8.2012(2) Å α= 90°
	b = 10.4016(2) Å β= 95.8770(10)°
	c = 17.8398(4) Å γ = 90°
Volume	1513.84(6) Å^3
Z	3
Density (calculated)	1.549 Mg/m^3
Absorption coefficient	1.300 mm^{-1}
F(000)	744
Crystal size	0.4 x 0.5 x 0.9 mm^3
Theta range for data collection	2.27 to 31.53°
Index ranges	-11<=h<=11, -14<=k<=14, -26<=l<=26
Reflections collected	22905
Independent reflections	4890 [R(int) = 0.0566]
Completeness to theta	31.53º, 96.7 %
Absorption correction	SADABS (Bruker-AXS)
Refinement method	Full-matrix least-squares on F^2
Data / restraints / parameters	4890 / 0 / 287
Goodness-of-fit on F^2	1.048
Final R indices [I>2sigma(I)]	R1 = 0.0330, wR2 = 0.0887
R indices (all data)	R1 = 0.0360, wR2 = 0.0909
Largest diff. peak and hole	0.750 and -0.819 e.Å^{-3}

Table S2. Selected geometric parameters for DFT optimized complexes [Cu^{II}(H33m)]$^{2+}$ (**1**) and [Ni^{II}(H33m)(CH$_3$CN)]$^{2+}$ (**3**).

	C-H	M-C	M-H$_a$	M-N1	M-N2	M-N3	M-NCCH$_3$	M-C-H$_a$	M-H$_a$-C	C4-C1-H$_a$	NBO donation (kJ/mol)	NBO retrodonation (kJ/mol)
Ligand H33m	1.084	-	-	-	-	-	-	-	-	179.0	-	-
[Cu^{II}(H33m)]$^{2+}$ (**1**)	1.099	2.171	2.140	2.086	2.046	2.087	-	73.7	76.8	161.8	102.4	9.1
[Ni^{II}(H33m)(CH$_3$CN)]$^{2+}$ (**3**)	1.098	2.266	2.243	2.154	2.077	2.154	2.042	74.8	77.1	167.8	110.5	9.7

Table S3. xyz coordinates for DFT optimized structures (B3LYP/6-31++G(d,p); vacuum, Gaussian03) of complexes (a) [Cu^{II}(H33m)]$^{2+}$ (**1**), (b) [Ni^{II}(H33m)(CH$_3$CN)]$^{2+}$ (**3**), (c) ligand H33m, (d) TS of complex **1** / TEMPO reaction, and (e) TS of water assisted reaction of complex **1** with TEMPO.

(a) [Cu^{II}(H33m)]$^{2+}$ (1) (doublet)

H	-4.909529	0.000260	-1.330784
C4	-3.990450	0.000302	-0.752298
H	-3.820937	2.156309	-0.786013
H	-3.821196	-2.155728	-0.785216
C	-3.385113	1.228361	-0.427309
C	-3.385265	-1.227697	-0.426855
H	-1.106957	2.568259	1.627417
H	-1.106635	-2.566666	1.628298
C	-2.222666	1.235765	0.337515
C	-2.222847	-1.234973	0.338040
H	1.241472	2.886855	1.369322
C	-1.312152	2.415379	0.562664
C1	-1.701417	0.000468	0.786549
C	-1.312528	-2.414711	0.563549
H	-1.708969	-3.350161	0.157760
H	-1.708023	3.350576	0.155730
H	1.240813	-2.887674	1.368726
H	3.075747	1.191332	1.152584
C	1.133309	2.947632	0.281460
H	0.875159	3.984367	0.034473
N3	-0.003240	2.058762	-0.109745
Cu^{II}	0.318382	-0.000527	-0.010784
N1	-0.003930	-2.059076	-0.110081
H	3.074398	-1.191556	1.152938
C	1.132755	-2.948020	0.280833
H	3.168400	3.337083	-0.206744
C	3.047383	1.231472	0.058611
H	0.874743	-3.984671	0.033388
C	2.434748	2.550549	-0.414084
H	-0.153305	2.188807	-1.114980
H	-0.154841	-2.189825	-1.115090
H	4.083946	1.166009	-0.292482

```
N     2.323729    0.000104   -0.414574
C     3.046808   -1.231549    0.058938
C     2.434210   -2.550429   -0.414438
H     2.308726    2.554006   -1.506197
H     3.167860   -3.337068   -0.207487
H     4.083650   -1.166282   -0.291364
H     2.383888   -0.000065   -1.437250
H     2.308270   -2.553328   -1.506563
Ha   -1.026308    0.000627    1.654033
```

(b) [Ni^{II}(H33m)(CH$_3$CN)]$^{2+}$ (3) (triplet)

```
H     4.944671    0.000060    0.410707
C     3.971822    0.000118   -0.071612
H     3.807154    2.155123   -0.037592
H     3.807213   -2.154902   -0.038218
C     3.338694    1.223384   -0.341750
C     3.338727   -1.223087   -0.342105
H     0.881531    2.545457   -2.192440
H     0.881661   -2.544694   -2.193230
C     2.105282    1.230370   -0.995453
C     2.105318   -1.229916   -0.995814
H    -1.359663    2.863626   -1.803832
C     1.192452    2.422075   -1.150071
C     1.550904    0.000276   -1.389486
C     1.192534   -2.421606   -1.150812
H     1.654650   -3.358944   -0.826710
H     1.654549    3.359335   -0.825712
H    -1.359633   -2.862716   -1.804898
H    -3.102574    1.168378   -1.537576
C    -1.219187    2.967653   -0.722718
H    -0.993336    4.022749   -0.526439
N    -0.049143    2.124871   -0.337255
Ni   -0.328689    0.000054   -0.124063
N    -0.049107   -2.124688   -0.337959
H    -3.102812   -1.167846   -1.537866
C    -1.219146   -2.967283   -0.723837
H    -3.245313    3.330406   -0.177353
C    -3.102269    1.225428   -0.443674
H    -0.993285   -4.022477   -0.528091
C    -2.495331    2.554786    0.012289
H     0.178154    2.360605    0.630841
H     0.178110   -2.360803    0.630061
H    -4.149560    1.171993   -0.122792
```

```
N    -2.397404   -0.000006    0.065716
C    -3.102320   -1.225283   -0.443985
C    -2.495279   -2.554794    0.011397
H    -2.339686    2.561470    1.100341
H    -3.245233   -3.330369   -0.178537
H    -4.149558   -1.171986   -0.122907
H    -2.518586   -0.000130    1.081172
H    -2.339584   -2.561925    1.099439
H     0.719953    0.000369   -2.106840
N     0.090348   -0.000275    1.874635
C     0.380008   -0.000812    2.996882
C     0.744214   -0.001239    4.405930
H    -0.159368    0.004106    5.023883
H     1.331596   -0.895711    4.636609
H     1.340851    0.887583    4.634695
```

(c) ligand H33m (singlet)

```
H     4.05590000   -1.49188400   -1.79749400
C     3.31256300   -1.11535800   -1.09979000
H     3.86405100    0.94669500   -1.39293800
H     2.51344700   -3.07121200   -0.65866200
C     3.20638500    0.25676900   -0.86800700
C     2.44503600   -2.00463900   -0.45639700
H     0.72041300   -3.50577000    0.77118700
H     2.46764400    2.78057200   -0.64099300
C     2.24838800    0.75489100    0.02806100
C     1.47825800   -1.52672500    0.43596000
H    -0.87714300   -1.79025100   -1.03929400
C     0.53340500   -2.48229700    1.14671000
C     1.40141400   -0.14816100    0.67849000
C     2.15086300    2.25533400    0.28033800
H     2.87270400    2.53493600    1.05961000
H     0.76937500   -2.49042500    2.21866500
H    -0.16642800    1.62482700   -0.74039500
H    -3.01418600   -0.42274100   -1.90886200
C    -1.45663900   -2.35853300   -0.30386000
H    -1.36390200   -3.42714500   -0.57599900
N    -0.87867500   -2.09795300    1.02209000
N     0.82872500    2.66951100    0.74462300
H    -2.70258100    2.07726900   -1.41877300
C    -0.22373500    2.61251000   -0.27578300
H    -3.48104400   -2.60457500   -1.04035700
```

C	-3.19468400	-0.49332100	-0.82527600
H	-0.07010600	3.35885000	-1.07784500
C	-2.93639200	-1.93635900	-0.36246100
H	-1.41443000	-2.60967500	1.71958200
H	0.88282000	3.59732700	1.15480500
H	-4.27056600	-0.27050900	-0.67733800
N	-2.32553300	0.46609900	-0.16307700
C	-2.67321200	1.86883600	-0.33884200
C	-1.62759300	2.76750200	0.33813700
H	-3.38418300	-2.08673900	0.63115100
H	-1.96675200	3.81055000	0.30001000
H	-3.68023200	2.11589200	0.05112400
H	-2.19083100	0.22804600	0.81600600
H	-1.56711200	2.49511400	1.40042100
H	0.64717800	0.23455400	1.35725900

(d) TS for reaction of [Cu^{II}(H33m)]$^{2+}$ (1) with TEMPO (singlet biradical)

H	0.231706	5.384544	-0.576282
C	0.342970	4.313371	-0.436392
H	0.423872	4.471555	1.714926
H	0.485724	3.920655	-2.554180
C	0.435897	3.795782	0.863663
C	0.469196	3.482645	-1.559570
H	-0.040135	1.178112	2.696650
H	0.100066	0.454227	-2.677962
C	0.585216	2.419564	1.036368
C	0.618168	2.108745	-1.373830
H	1.032699	-0.828084	3.234215
C	0.846257	1.722947	2.351059
C	0.592916	1.556926	-0.078263
C	0.950892	1.109901	-2.457082
H	1.260007	1.577440	-3.398688
H	1.146172	2.407650	3.152145
H	1.329592	-1.542117	-2.768596
H	1.852790	-2.657735	1.685721
C	2.008409	-0.332908	3.177261
H	2.186658	0.153549	4.144696
N	1.919493	0.693387	2.103062
Cu	1.798806	0.047340	0.135982
N	2.047596	0.229800	-1.914941
H	2.016980	-2.948190	-0.796656
C	2.278209	-0.995569	-2.725862
H	3.172940	-2.017564	3.772084

```
C     2.869190   -2.247706    1.673782
H     2.542533   -0.718920   -3.754395
C     3.104769   -1.360167    2.898137
H     2.807997    1.204578    2.097792
H     2.906219    0.788081   -1.960641
H     3.560758   -3.098787    1.703601
N     3.049443   -1.531188    0.368394
C     3.019796   -2.506693   -0.769902
C     3.367289   -1.883158   -2.123796
H     4.085681   -0.866854    2.827369
H     3.552651   -2.703502   -2.826094
H     3.723576   -3.319354   -0.551535
H     4.002640   -1.154017    0.386404
H     4.318726   -1.334714   -2.057904
H    -0.572560    0.504710    0.150047
O    -1.206139   -0.365683    0.462018
N    -2.410059   -0.535897   -0.071969
C    -3.432575    0.563338    0.119616
C    -4.680035    0.250609   -0.737520
H    -5.471208    0.929204   -0.401820
H    -4.466018    0.514047   -1.781406
C    -5.139316   -1.204930   -0.676250
H    -5.455172   -1.481447    0.336355
H    -6.017517   -1.336638   -1.315984
C    -4.008981   -2.105404   -1.171489
H    -3.787505   -1.856088   -2.217374
H    -4.306127   -3.159369   -1.158038
C    -2.709599   -1.992287   -0.344333
C    -3.775098    0.624829    1.627829
H    -2.871706    0.748973    2.231313
H    -4.308360   -0.263363    1.972577
H    -4.421767    1.491668    1.795021
C    -2.836045    1.903672   -0.334484
H    -2.448260    1.847083   -1.356027
H    -2.051707    2.266783    0.332013
H    -3.640026    2.645622   -0.327920
C    -2.830687   -2.728096    1.010967
H    -1.943610   -2.562504    1.628164
H    -2.918969   -3.800740    0.813210
H    -3.713117   -2.419058    1.575030
C    -1.536176   -2.574489   -1.151788
H    -0.618636   -2.624349   -0.559847
H    -1.352804   -1.989724   -2.060037
H    -1.799747   -3.591015   -1.458241
```

(e) TS for water assisted reaction of [Cu^{II}(H33m)]$^{2+}$ (1) with TEMPO (singlet biradical)

H	1.436128	1.880030	-3.096334
C	1.220208	1.171414	-2.302235
H	2.095203	2.420671	-0.774966
H	0.467396	-0.323414	-3.664568
C	1.580422	1.486629	-0.984089
C	0.655716	-0.071040	-2.624333
H	0.952693	0.926843	2.142135
H	-1.127829	-2.520259	-1.510796
C	1.306644	0.570506	0.030043
C	0.385137	-0.978407	-1.601389
H	1.454579	-0.623452	3.790898
C	1.777419	0.682687	1.461204
C	0.633757	-0.633502	-0.258371
C	-0.073706	-2.404823	-1.789440
H	0.039419	-2.761617	-2.819428
H	2.550714	1.445846	1.603164
H	-0.875627	-4.465570	-0.258261
H	0.910669	-3.075963	3.785353
C	2.435151	-0.824622	3.345093
H	3.130708	-0.068398	3.730312
N	2.289627	-0.675152	1.871291
Cu	1.247417	-2.135708	0.823109
N	0.733045	-3.261633	-0.844475
H	-0.055978	-4.656189	2.117986
C	0.143991	-4.611480	-0.632103
H	3.091642	-2.221199	4.816716
C	1.914688	-3.349331	3.441290
H	0.067721	-5.139869	-1.590979
C	2.908969	-2.223868	3.736348
H	3.226503	-0.760558	1.464271
H	1.646078	-3.395801	-1.290506
H	2.210163	-4.251060	3.991635
N	1.811422	-3.693593	1.985043
C	0.960112	-4.913608	1.797746
C	0.953881	-5.443357	0.361965
H	3.883514	-2.444365	3.275794
H	0.518527	-6.448647	0.384611
H	1.322276	-5.697870	2.473844
H	2.756460	-3.964620	1.694430
H	1.984333	-5.579787	0.001404

H	-2.452610	-1.204974	0.544710
O	-3.268680	-1.672284	-0.399781
N	-4.550559	-1.439573	-0.478613
C	-5.382779	-1.674462	0.760515
C	-6.799702	-1.097430	0.550283
H	-7.427112	-1.477843	1.363747
H	-6.758688	-0.006840	0.670727
C	-7.409174	-1.418757	-0.813899
H	-7.552904	-2.498423	-0.940779
H	-8.404720	-0.968658	-0.882915
C	-6.510791	-0.845650	-1.909080
H	-6.465940	0.245314	-1.795202
H	-6.927197	-1.037981	-2.903655
C	-5.072453	-1.406764	-1.897780
C	-5.418461	-3.195073	1.030562
H	-4.404020	-3.603798	1.062112
H	-5.988870	-3.737893	0.273539
H	-5.893621	-3.373125	2.000406
C	-4.724449	-0.954075	1.949557
H	-4.537148	0.101404	1.719210
H	-3.797457	-1.435976	2.270842
H	-5.415507	-0.984106	2.797043
C	-5.015961	-2.837906	-2.474565
H	-4.012857	-3.259776	-2.365350
H	-5.257784	-2.798165	-3.541098
H	-5.731748	-3.510012	-1.995112
C	-4.154988	-0.476088	-2.709631
H	-3.145409	-0.880606	-2.808121
H	-4.095091	0.516300	-2.250858
H	-4.577742	-0.357670	-3.711859
H	-0.597603	-0.821149	0.584143
O	-1.599565	-0.857101	1.177731
H	-1.808730	0.042163	1.492035
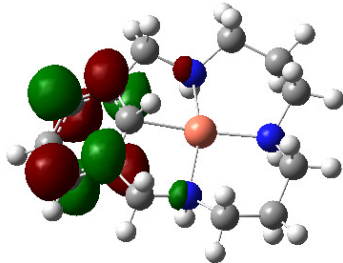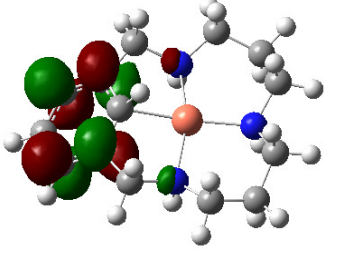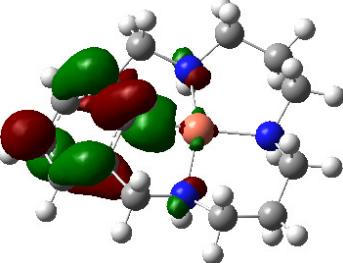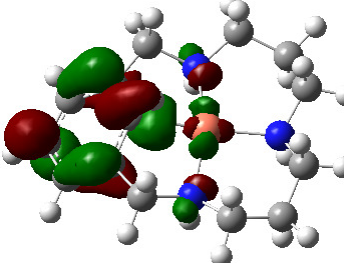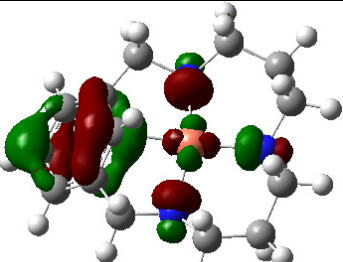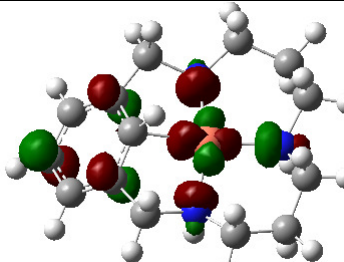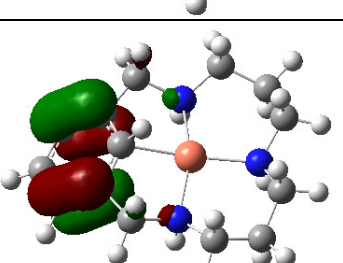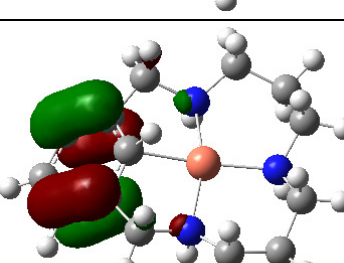
Table S4. Kinetic parameters for the for C-H$_a$ cleavage reactions of **1** and **3**, and the respective mono-deuterated D-H33m systems at 286 K monitored by UV-Vis. (1.3:1 ligand:M^{II} molar ratio (M = Cu, Ni), anhydrous and anaerobic in CH$_3$CN).
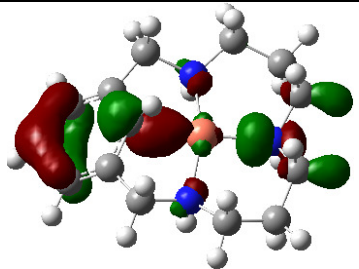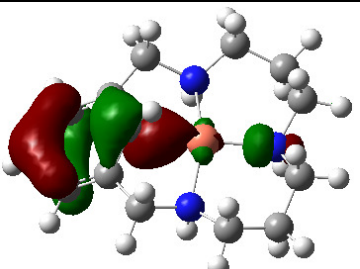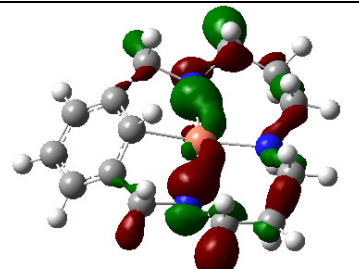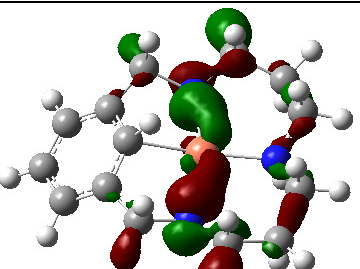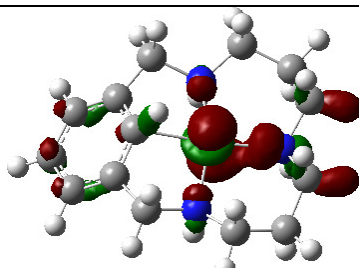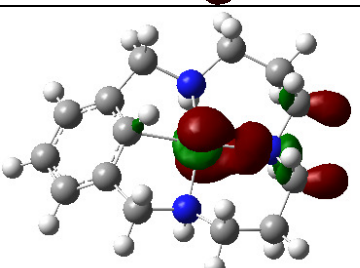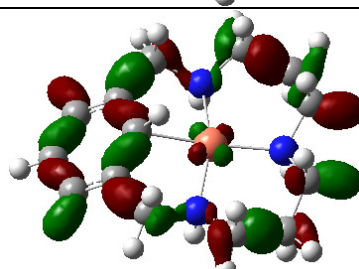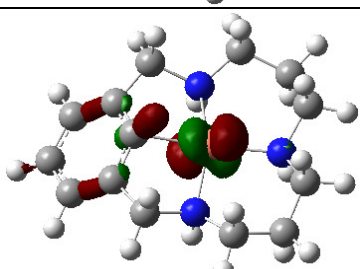
	k_{obs} (s^{-1})
[Cu^{II}(H33m)]$^{2+}$ (1)	0.142 (1)[a]
[Cu^{II}(D-H33m)]$^{2+}$	0.055 (1)[a]
[Ni^{II}(H33m)(CH$_3$CN)]$^{2+}$ (3)	0.000090 (1)[b]
[Ni^{II}(D-H33m)(CH$_3$CN]$^{2+}$	0.0000076(1)[b]

[a] k_{obs} was determined in each case from a single exponential fit to the absorption decay at 425 nm (r^2 > 0.99, [Cu^{II}] = 1.25 mM). [b] k_{obs} was determined in each case from a single exponential fit to the absorption growth at 400 nm (r^2 > 0.99 , [Ni^{II}] = 2.5 mM).
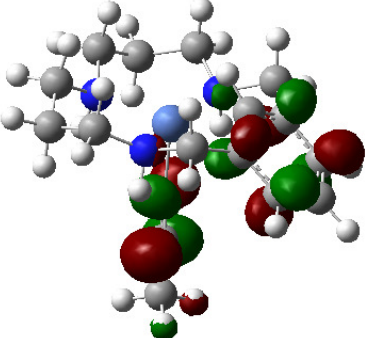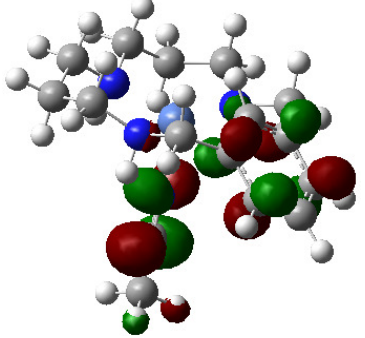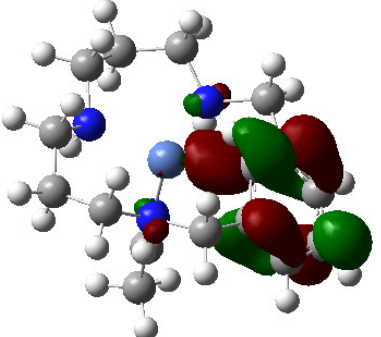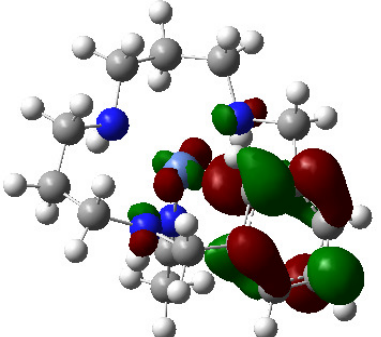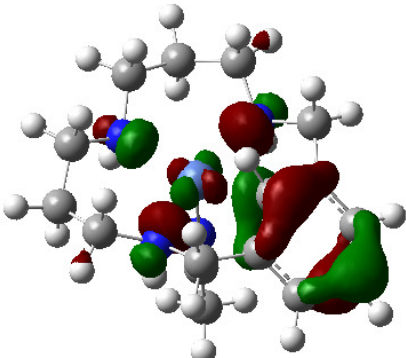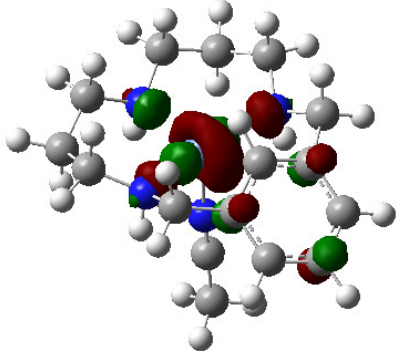
Table S5. Important molecular orbitals (MOs) and energies (a.u.) (Gaussian03, B3LYP/6-31++G(d,p)) for a) **1** and b) **3**.
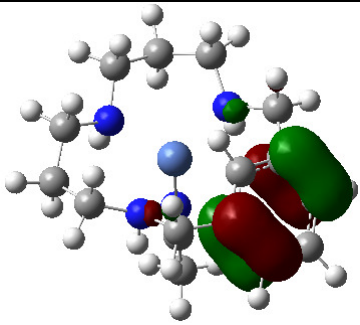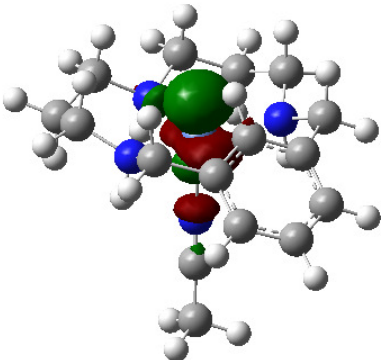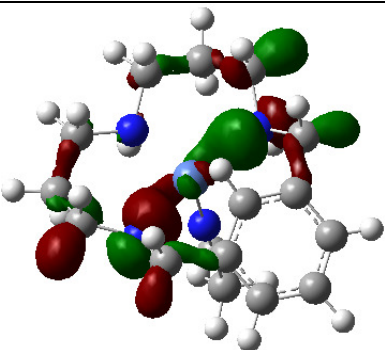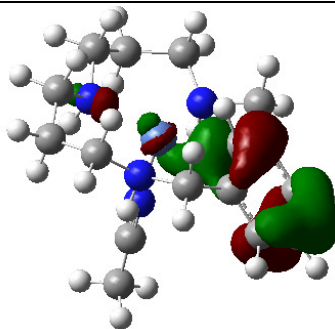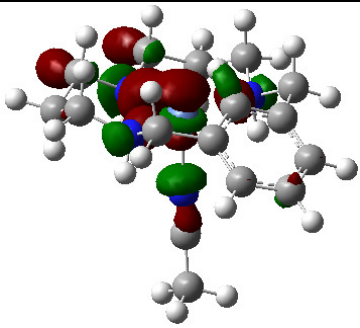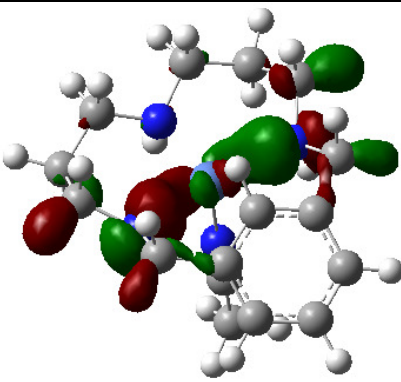
a)

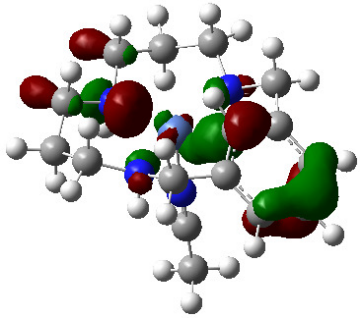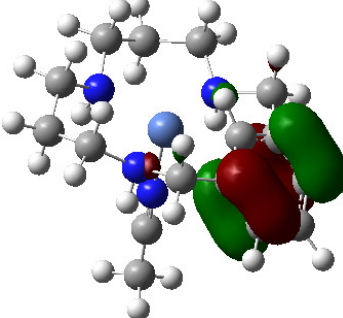| [Cu^{II}(H33m)]$^{2+}$ (**1**)	α		β	
80		-0.270		-0.267
79		-0.307		-0.293
78 (SOMO)		-0.488		-0.385
77		-0.514		-0.511

76		-0.544		-0.528
75		-0.566		-0.557
74		-0.581		-0.567
73		-0.592		-0.585

b)

[Ni^{II}(H33m)(CH$_3$CN)]$^{2+}$ (**3**)	α	β
91	-0.257	-0.256
90	-0.280 (LUMO)	-0.269
89	-0.475 (HOMO)	-0.338

88	-0.493	-0.358 (LUMO)
87	-0.517	-0.491 (HOMO)
86	-0.536	-0.501
85	-0.556	-0.526
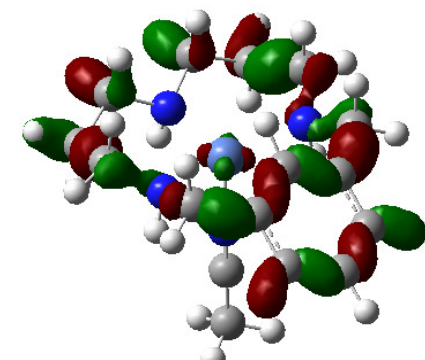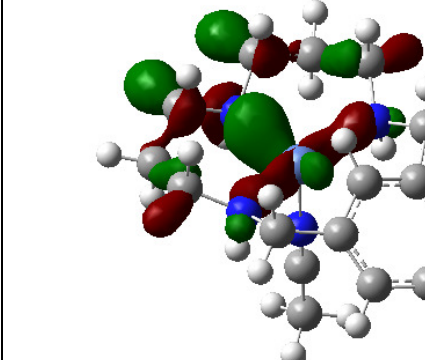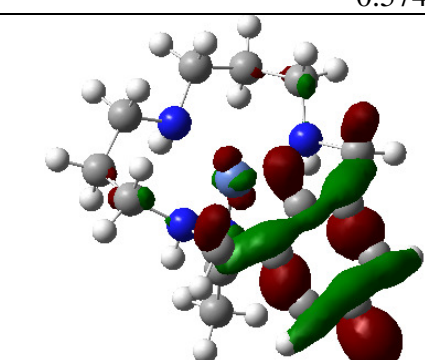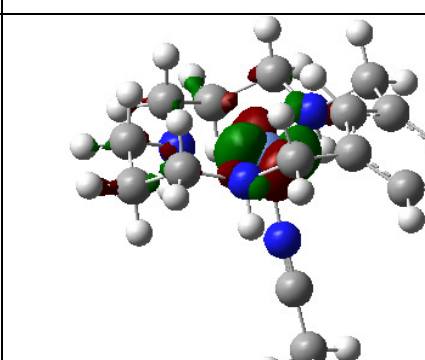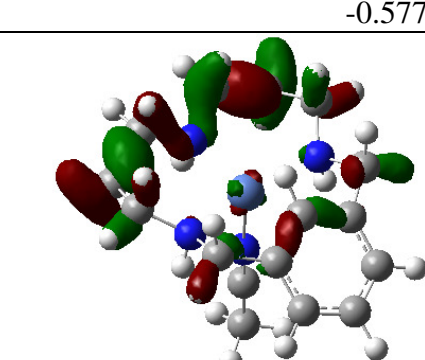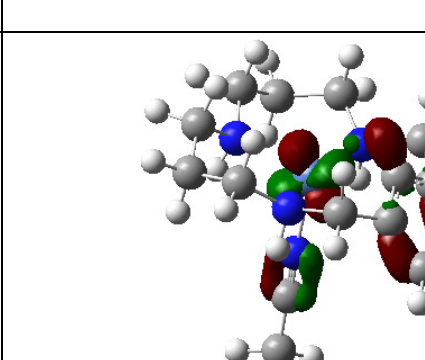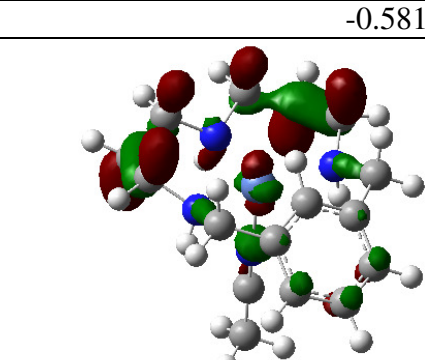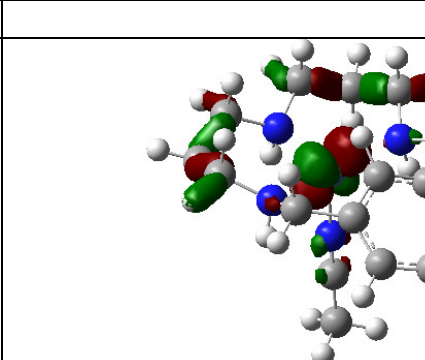
84	-0.574	-0.546
83	-0.577	-0.561
82	-0.581	-0.565
81	-0.588	-0.570

Table S6. Theoretically predicted electronic spectra using TD-DFT calculations of for **1** and **3**. Experimental values are compared with theoretical λ_{max} (relative intensities in parenthesis), and correlated with the corresponding departure and arrival orbitals of each transition. Relevant orbitals depicted in Table S5.

Complex **1**				Complex **3**			
$\lambda\,(\varepsilon(M^{-1}\cdot cm^{-1}))_{exp}$	λ_{theor} (relative intensity)	MO's implied	Type	$\lambda(\varepsilon(M^{-1}\cdot cm^{-1}))_{exp}$	λ_{theor}(relative intensity)	MO's implied	Type
272 (4060)	290 (0.015)	73β→78β 74β→78β 77α→80α 77β→80β	d-d π-π	-	285 (0.045) 294 (0.058)	88α→89α 89α→90α 87β→91β 81β→89β 85β→89β	π-π d-d
324 (8500)	351 (0.118)	78α→79α	π-π	325 (sh, 180)	306 (0.0949)	86β→89β	π-d
425 (960)	457 (0.125)	76β→78β	π-d	385 (sh, 92)	347 (0.033)	84β→88β	d-d
640 (185)	525 (0.015)	77β→78β	π-d	600 (27)	660 (0.006)	83β→89β	d-d

5. SUPPLEMENTARY REFERENCES

[1] X. Ribas, D. A. Jackson, B. Donnadieu, J. Mahía, T. Parella, R. Xifra, B. Hedman, K. O. Hodgson, A. Llobet, T. D. P. Stack, *Angew. Chem. Int. Ed.*, **41**, 2991 (2002)

[2] R. Xifra, X. Ribas, A. Llobet, A. Poater, M. Duran, M. Solà, T. D. P. Stack, J. Benet-Buchholz, B. Donnadieu, J. Mahía, T. Parella, *Chem. Eur. J.*, **11**, 5146 (2005)

[3] X. Ribas, R. Xifra, T. Parella, A. Poater, M. Solà, A. Llobet, *Angew. Chem. Int. Ed.*, **45**, 2941 (2006)

[4] S. Stoll, A. Schweiger, *J. Mag. Res,.* **178**, 42 (2006)

[5] Z. L. Madi, S. Van Doorslaer, A. Schweiger, *J. Mag. Res.,* **154**, 181 (2002)

[6] A. D. Becke, *J. Chem. Phys.*, 98, 5648 (1993)

[7] C. Lee, W. Yang, R. G. Parr, *Phys. Rev. B*, **37**, 785 (1988)

[8] P. J. Stevens, F. J. Devlin, C. F. Chabalowski, M. J. Frisch, *J. Phys. Chem.*, **98**, 11623 (1994)

[9] M. W. Schmidt, K. K. Baldridge, J. A. Boatz, S. T. Elbert, M. S. Gordon, J. H. Jensen, S. Koseki, N. Matasunaga, K. A. Nguyen, S. J. Su, T. L. Windus, M. Dupuis, J. A. Montgomery, *J. Comput. Chem.*, **14**, 1347 (1993)

[10] M. J. Frisch, G. W. Trucks, H. B. Schlegel, G. E. Scuseria, M. A. Robb, J. R. Cheeseman, J. Montgomery, T. Vreven, K. N. Kudin, J. C. Burant, J. M. Millam, S. S. Iyengar, J. Tomasi, V. Barone, B. Mennucci, M. Cossi, G. Scalmani, N. Rega, G. A. Petersson, H. Nakatsuji, M. Hada, M. Ehara, K. Toyota, R. Fukuda, J. Hasegawa, M. Ishida, T. Nakajima, Y. Honda, O. Kitao, H. Nakai, M. Klene, X Li, J. E. Knox, H. P. Hratchian, J. B. Cross, C. Adamo, J. Jaramillo, R. Gomperts, R. E. Stratmann, O. Yazyev, A. J. Austin, R. Cammi, C. Pomelli, J. W. Ochterski, P. Y. Ayala, K. Morokuma, G. A. Voth, P. Salvador, J. J. Dannenberg, V. G. Zakrzewski, S. Dapprich, A. D. Daniels, M. C. Strain, O. Farkas, D. K. Malick, A. D. Rabuck, K. Raghavachari, J. B. Foresman, J. V. Ortiz, Q. Cui, A. G. Baboul, S. Clifford, J. Cioslowski, B.B. Stefanov, G. Liu, A. Liashenko, P. Piskorz, I. Komaromi, R. L. Martin, D. J. Fox, T. Keith, M. A. Al-Laham, C. Y. Peng, A. Nanayakkara, M. Challacombe, P. M. W. Gill, B. Johnson, W. Chen, M. W. Wong, C. Gonzalez, J. A. Pople, Gaussian 03, revision C02; Wallingford, CT, 2004.

[11] J. Tomasi, M. Persico, *Chem. Rev.*, **94**, 2027 (1994)

[12] V. Barone, M. Cossi,*J. Phys. Chem. A*, **102**, 1995 (1998).

[13] A. E. Reed, L. A. Curtis, F. Weinhold, *Chem. Rev.*, **88**, 899 (1988)

[14] a) J. Kruszewski, T. M. Krygowski, *Tetrahedron Lett.*, **13**, 3839 (1972). b) Krygowski, T. M. *J. Chem. Inf. Comp. Sci.*, **33**, 70-78 (1993)

[15] a)T. M. Krygowski, M. K. Cyrański, *Chem. Rev.*, **101**, 1385 (2001). b) P. v. R. Schleyer, *Chem. Rev.*, **101**, 1115 (2001)

[16] P. v. R. Schleyer, C. Maerker, A. Dransfeld, H. Jiao, N. J. R. van Eikema Hommes, *J. Am. Chem. Soc.*, **118**, 6317 (1996)

[17] P. v. R. Schleyer, M. Monoharar, Z. Wang, B. Kiran, H. Jiao, R. Puchta, N. J. R. van Eikema Hommes, *Org. Lett.*, **3**, 2465 (2001)

[18] Velde, G. T.; Bickelhaupt, F. M.; Baerends, E.J.; Fonseca Guerra, C.; van Gisbergen, S. J. A.; Snijders, J. G.; Ziegler, T. *J. Comput. Chem.* **2001**, *22*, 931-967

[19] a) Becke, A. D. *Phys. Rev. A* **1998**, *38*, 3098-3100. b) Perdew, J. R.; Burke, K.; Wang. Y. *Phys. Rev B* **1996**, *54*, 16533-16539

[20] E. van Lenthe, J. G. Snijders, E. J. Baerends, *J. Chem. Phys.,* **105**, 6505 (1996)

[21] R. S. Drago, *Physical Methods for Chemists, 2nd Ed.* (Surfside Scientific Publishers, Gainesville, 1992)

[22] J. C. Ianni, *Kintecus*, version 3.95, 2008, www.kintecus.com

[23] P. Atkins, J. De Paula, *Physical Chemistry* (Oxford University Press, Oxford, 2006)

[24] X. Chen, X.-S. Hao, C. E. Goodhue, J.-Q. Yu, *J. Am. Chem. Soc.*, **128**, 6790 (2006)